Point-contact spectroscopy

1989 J. Phys.: Condens. Matter 1 3157

(http://iopscience.iop.org/0953-8984/1/20/001)

J. Phys.: Condens. Matter. 1 (1989) 3157–3189. Printed in the UK

REVIEW ARTICLE

Point-contact spectroscopy

A M Duif, A G M Jansen and P Wyder
Max-Planck-Institut für Festkörperforschung, Hochfeld-Magnetlabor, 25 Avenue des Martyrs, 166 X, F-38042 Grenoble Cédex, France

Received 18 March 1988, in final form 10 October 1988

Abstract. Micro-contacts between metals at low temperatures reveal non-linear structures in the current–voltage characteristics. These deviations from Ohm's law allow an energy-resolved spectroscopy of the interaction of the conduction electrons with elementary excitations (e.g. phonons) in a metal. To explain the method, the important parameters (electron mean free path versus contact dimension) in point-contact spectroscopy will be discussed together with examples of spectroscopic information obtained in various systems. Local temperature gradients in the contact region offer the possibility to study thermo-electric phenomena in small constrictions, such as thermal voltages in non-homogeneous contacts and quenching of the phonon-drag term in the thermo-power in homogeneous contacts. Besides these aspects of the point-contact technique, recent experiments will be shown with applications of point contacts other than just spectroscopy: magneto-resistance of a point contact, high-frequency rectification with a point contact as the non-linear element, electron focusing using a double point-contact set-up, electrical noise in constrictions and generation of phonons by means of point contacts.

1. Introduction

Point-contact spectroscopy nowadays has become a well established technique in the study of the interaction mechanisms of electrons with all kinds of elementary excitations in metals. Small constrictions between two metals show deviations from Ohm's law. The non-linearity is a measure of the inelastic scattering of the conduction electrons, where the applied voltage defines the energy scale for the interaction process. Those non-linearities in the current–voltage characteristics were discovered by Yanson, who examined the I–V characteristics of shorted metal–insulator–metal (MIM) tunnel junctions (Yanson 1974). In the second derivative d^2V/dI^2 of the voltage V with respect to the current I, he found structures which turned out to coincide with the Eliashberg function α^2F for the electron–phonon interaction. This Yanson experiment was the start of a whole series of experiments in which mainly the electron–phonon interaction was studied in all kinds of materials. But also other scattering mechanisms of electrons were observed in point-contact experiments, like e.g. electron–magnetic impurity interaction and electron–magnon interaction.

Although point-contact experiments with superconductors show interesting features, we will restrict ourselves to point-contact experiments on normal (N–N) contacts. In this review paper we will not give a detailed description of the complete point-contact theory but only give the main results. For a complete theory on point contacts in the ballistic regime we shall refer to Kulik *et al* (1977) and Jansen *et al* (1980). For a theory

0953-8984/89/203157 + 33 $02.50

on point contacts in the dirty limit we refer to Kulik and Yanson (1978). We will also not give a complete survey on all the possible materials that have been studied during the last few years. For reviews on this see Yanson (1983) and Yanson and Shklyarevskii (1986). Here we will discuss the possibilities of the technique and a number of new interesting experiments that have been performed during the last few years.

In the first part of this review attention is focused on the spectroscopic side of the point-contact technique. Here the aim is to obtain an energy-resolved determination of the inverse scattering time $1/\tau$ of electrons with elementary excitations in the metal. The important criteria in a point-contact experiment will be explained and illustrated with typical examples of spectroscopic applications, which also show the limitations of this technique. The understanding of point-contact spectroscopy has initiated experiments dealing with aspects other than just spectroscopy, exploiting the small dimension of the contact. A considerable number of experiments of this kind have been performed during the last few years, for instance those dealing with thermal conductivity, with the quenching of phonon drag in the thermo-power of point contacts, with thermo-electric effects, those on double point contacts and on point contacts in magnetic fields.

2. Characterisation of a point contact

There are three methods of fabricating a point contact between two metals. The first point contacts that existed were a short circuit in a MIM tunnel junction. The method was extended by the so-called pressure-type contacts in which a sharp whisker is pressed on a flat surface. With this technique it was easier to control the diameter of the contact, which is an important parameter in the experiments. These spear–anvil contacts made the point-contact technique accessible for the study of a large number of materials. The newest method is just pressing together two sharp edges of two bulk pieces of metal. Besides the advantage of the pressure-type contacts, now even single-crystal contacts could be made.

The two typical lengths for the characterisation of the contact problem are the electron mean free path l and the radius a of the constriction. Actually the mean free path involves an elastic mean free path l_e and an inelastic one, $l_i(\varepsilon)$. The inelastic mean free path depends on the electron energy $\varepsilon = eV$ with respect to the Fermi level. Comparing these typical lengths with each other, three regimes are possible.

The first regime is the ballistic regime in which the electron mean free path l is much larger than the contact dimension a. In this regime an applied voltage will accelerate the electrons within the distance of a mean free path. Thus the electrons will then pass through the contact ballistically, gaining an energy eV, where V is the applied voltage over the contact. The problem can be treated analogously to the problem of the flow of a dilute gas through a small hole (Knudsen 1934). Sharvin realised the peculiar transport of current through such a contact in the ballistic regime and calculated the resistance (Sharvin 1965). He found a resistance $R_S = 4\rho l/3\pi a^2$, where ρ is the resistivity of the material under study. This expression for the Sharvin resistance R_S is independent of the electron mean free path.

The opposite case of this ballistic regime is the dirty, thermal, or Maxwell regime, where the mean free path of the electrons is much smaller than the contact radius a. For this regime the Poisson equation can be solved using the proper boundary conditions, leading to a resistance $R_M = \rho/2a$, already calculated by Maxwell (1904). In contrast with the ballistic regime, where the electrons lose their energy over a rather large distance

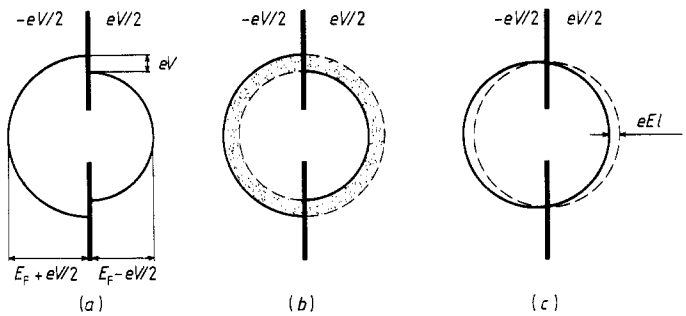

Figure 1. Distribution of the electronic energy at the centre of the contact for an applied voltage V over a point contact in (*a*) ballistic, (*b*) diffusive and (*c*) thermal regimes.

from the constriction, in this regime they lose their energy in the contact area itself. Therefore this Joule heating leads to an increase of temperature at the centre of the contact.

When one is not in one of these two limits, one could easily expect some interpolation of the two limiting resistances (Wexler 1966):

$$R = \frac{4\rho l}{3\pi a^2} + \Gamma(K)\frac{\rho}{2a} = \frac{4\rho l}{3\pi a^2}\left(1 + \frac{3\pi}{8}\Gamma(K)\frac{a}{l}\right). \tag{1}$$

Here $K = l/a$ is the Knudsen number and $\Gamma(K)$ is a slowly varying function of the order of unity.

The third possible regime is the so-called diffusive regime. This is the regime where the elastic mean free path l_e of the electrons is small compared with the contact dimension but where the diffusion length $\Lambda = (l_i l_e)^{1/2}$ for inelastic scattering is still bigger than the contact dimension. In this case still no heating occurs in the contact area.

Figure 1 shows the difference in the electron distribution functions at the centre of the contact for the three regimes. In figure 1(*a*) the deformed Fermi spheres are depicted for the ballistic regime. Since there is ballistic flow of electrons from both sides of the contact, the Fermi sphere consists of two half-spheres with a difference in radius equal to the applied energy eV. The picture for the diffuse regime (figure 1(*b*)) differs from the 'ballistic picture' because the elastic scattering redistributes the electrons isotropically over the Fermi sphere, but still in an energy shell with a width given by the applied voltage (dotted area). Since there is still more electrons in the left half-sphere than in the right one, there is a net flow of electrons from the right to the left. Figure 1(*c*) just shows the shifted Fermi sphere which is valid for a point contact in the thermal regime, as is normal for the uniform transport of electrons in a conductor. Because of strong inelastic scattering the shift in energy space will be smaller than the applied voltage. In the next section we will show how these three different micro-contact regimes manifest themselves in the experiments and how the observed non-linearities can be explained theoretically.

3. Non-linearities observed with point contacts

3.1. Ballistic regime

In the ballistic point-contact regime, direct energy-resolved information is obtained about the inelastic scattering of the electrons in the contact region. Figure 2 shows a

pronounced example of the information obtained with point contacts. This figure shows the current–voltage characteristic and its derivatives of a Cu–Cu point contact in the ballistic regime, measured at liquid-helium temperatures. The broken curve in figure 2(*c*) represents the phonon density of states $F(\varepsilon)$ obtained with neutron scattering experiments. There is a clear resemblance between this curve and the measured second derivative $\mathrm{d}^2V/\mathrm{d}I^2$. For an interpretation of this result it is necessary to solve the Boltzmann equation for the point-contact problem. This can be done iteratively. The zeroth-order solution describes the ballistic injection of electrons without any scattering and yields the expression for the Sharvin resistance. The first-order solution describes the inelastic scattering of the injected electrons, back through the orifice. This first-order correction $I^{(1)}$ to the total current leads to a correction of the order of $a/l(\varepsilon)$ in the resistance, analogously to the second term in equation (1). This correction $I^{(1)}$ to the total current is given by

$$I^{(1)} = -\frac{2\pi e}{\hbar}\Omega_{\mathrm{eff}} N(0) \int_0^{eV} \mathrm{d}\varepsilon \int_0^{\varepsilon} \mathrm{d}\varepsilon'\, S(\varepsilon - \varepsilon'). \tag{2}$$

Here $N(0)$ is the density of states at the Fermi level, Ω_{eff} is a kind of effective volume in which the inelastic scattering of electrons that contribute to $I^{(1)}$ takes place, and $S(\varepsilon)$ is the spectral function for the concerned interaction. This spectral function $S(\varepsilon)$ consists of an integration over all initial and final electron states $|\boldsymbol{k}\rangle$ and $|\boldsymbol{k}'\rangle$ of the scattering matrix elements $|g_{kk'}|$ and an efficiency function $\eta(\boldsymbol{k}, \boldsymbol{k}')$:

$$S(\varepsilon) = \frac{N(0)}{32\pi^2} \int \frac{\mathrm{d}^2\boldsymbol{k}}{k^2} \int \frac{\mathrm{d}^2\boldsymbol{k}'}{k'^2} |g_{kk'}|^2\, \eta(\boldsymbol{k}, \boldsymbol{k}')\, \delta(\varepsilon - \varepsilon_k + \varepsilon_{k'}). \tag{3}$$

The efficiency function $\eta(\boldsymbol{k}, \boldsymbol{k}')$ is the normalised common volume of two cylinders through the boundary of the orifice, one parallel to $\boldsymbol{k}$ of the incoming electron and the other parallel to $\boldsymbol{k}'$ of the inelastic scattered electron. Retaining only the angular dependence in the scattering event, the efficiency can be written as $\eta(\theta) = (1 - \theta/\tan\theta)/2$ (van Gelder 1980), analogously to the function $(1 - \cos\theta)$ in the electrical transport problem. The effective volume in the ballistic regime is given by $\Omega_{\mathrm{eff}} = 8a^3/3$.

The expression for the differential conductivity $\mathrm{d}I/\mathrm{d}V$ is now given by

$$\frac{\mathrm{d}I}{\mathrm{d}V} = \frac{1}{R_S} - \tfrac{2}{3}e^2a^3N(0)\frac{1}{\tau(eV)}. \tag{4}$$

This inverse scattering time $1/\tau(eV)$ of an electron with energy eV above the Fermi level is related to the spectral function $S(\varepsilon)$ via

$$\frac{1}{\tau(eV)} = \frac{2\pi}{\hbar}\int_0^{eV} S(\varepsilon)\,\mathrm{d}\varepsilon. \tag{5}$$

The second derivative $\mathrm{d}^2I/\mathrm{d}V^2$ of the current with respect to the voltage is directly proportional to the spectral function $S(\varepsilon)$ since

$$\frac{\mathrm{d}^2I}{\mathrm{d}V^2} = -\frac{2\pi e^3}{\hbar}\Omega_{\mathrm{eff}} N(0)\, S(eV) \tag{6}$$

and thus a direct measurement of the spectral function $S(eV)$ is possible. For the case of electron–phonon interaction as in figure 2, the spectral function $S(\varepsilon)$ is the well

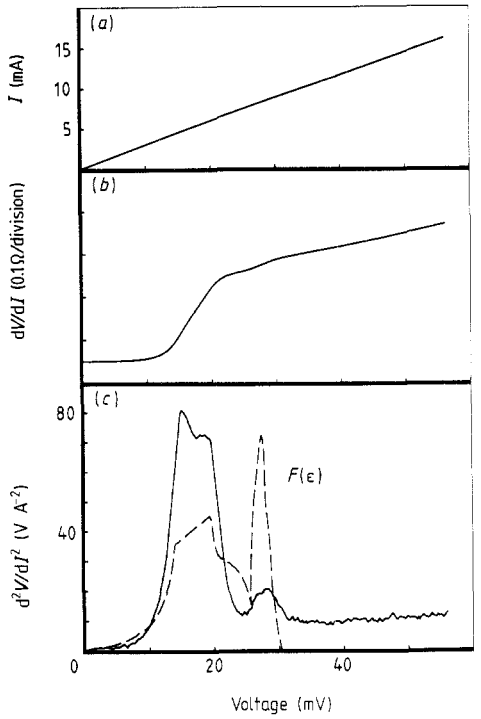

Figure 2. Measured (*a*) current–voltage characteristic, (*b*) differential resistance dV/dI and (*c*) second derivative d^2V/dI^2 for a Cu–Cu point contact with resistance $R_0 = 3.3\,\Omega$ at temperature 1.5 K. The broken curve in (*c*) represents the phonon density of states $F(\varepsilon)$ obtained from neutron scattering experiments.

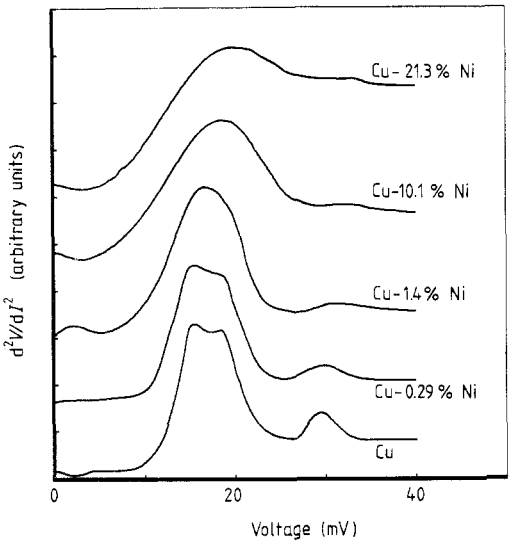

Figure 3. Measured point-contact spectra d^2V/dI^2 for point contacts consisting of pure Cu and some CuNi alloys, showing the transition from the ballistic to the diffusive regime. By increasing the Ni concentration the Knudsen ratio l_e/a goes from 29 to 0.07. The spectra were measured at $T = 4.2$ K. (After Lysykh *et al* (1980).)

known Eliashberg function $\alpha^2F(\varepsilon)$ with, as a slight modification, the efficiency function $\eta(\boldsymbol{k}, \boldsymbol{k}')$ mentioned above. This method of obtaining phonon spectra has been used extensively during the last few years. For many (normal) metals it was the first method to give the detailed energy dependence of the electron–phonon interaction function $\alpha^2F(\varepsilon)$. For a complete review on the investigation of the electron–phonon interaction by means of point contacts, we refer to Yanson (1983).

In measurements on the point-contact electron–phonon interaction function $\alpha^2F_p(\varepsilon)$, often a considerable background is found (Jansen *et al* 1980). One expects the function α^2F_p to be zero above the Debye energy, which owing to equation (6) should lead to $d^2I/dV^2 = 0$ for these energies. The fact that this does not occur is generally understood to be due to the presence of non-equilibrium phonons in the system. This leads to an additional scattering of the electrons with these non-equilibrium phonons and therefore to a background signal which is not included in the theory. The background signal is a smooth signal which is zero at zero energy, increases smoothly at the phonon energies and saturates above the maximum phonon energy. This background signal $B(eV)$ is best described by the integral

$$B(eV) = \kappa \int_0^{eV} [\alpha^2F_p(\varepsilon)/\varepsilon]\,d\varepsilon$$

where κ is some constant. Thus the measured signal is commonly believed to be

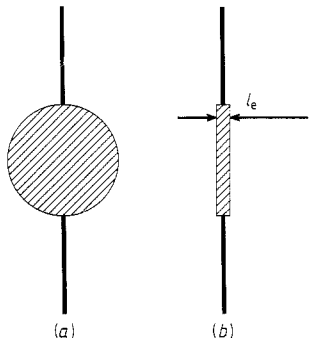

Figure 4. Schematic representation of the effective volume Ω_{eff} of a point contact in (*a*) the ballistic regime and (*b*) the diffusion regime.

$$\frac{d^2I}{dV^2} = \text{constant} \times \left(\alpha^2 F_p(eV) + \kappa \int_0^{eV} \frac{\alpha^2 F_p(\varepsilon)}{\varepsilon} d\varepsilon \right). \tag{7}$$

This assumption gives us the possibility to correct for the background and to determine the point-contact electron–phonon interaction function $\alpha^2 F_p(\varepsilon)$.

3.2. Diffusive regime

In the diffusive point-contact regime it is still possible to obtain direct energy-resolved information about the inelastic scattering of the electrons as in the ballistic regime. Figure 3 shows very nicely the transition from a point contact in the ballistic regime to a point contact in the diffusive regime (Lysykh *et al* 1980). The lowest curve represents the phonon spectrum of a pure Cu–Cu point contact. Adding Ni to the sample (other curves) reduces the elastic mean free path of the electrons in the material under study and brings the point contacts into the diffusive regime. The most striking features of these curves are the reduction of the signal, the broadening of the spectra and a shift of the phonon peaks to higher energies. For a theoretical understanding we still can use equations (2)–(6). The spectral function $S(\varepsilon)$, however, now contains another efficiency function $\eta(\boldsymbol{k}, \boldsymbol{k}')$, in which the demands on momentum conservation are less stringent because of the elastic scattering (Kulik and Yanson 1978). This explains the different shape of the measured spectral function in this diffusive regime compared with the one measured in the ballistic regime. The reduction of the signal can be explained with the effective volume Ω_{eff}. In the diffusive regime this effective volume is given by $\Omega_{\text{eff}} = \pi a^2 l_e/4$, where l_e is the elastic mean free path. The effective volumes are sketched schematically in figure 4. Figure 4(*a*) shows the effective volume for a point contact in the ballistic regime except for a pre-factor. If an inelastic scattering process takes place outside this volume, the chance of the electron flowing back through the orifice becomes very small because of the small solid angle $\Omega(\boldsymbol{r})$ the orifice subtends from that point. Therefore inelastic scattering processes outside this volume hardly contribute to the back-flow current $I^{(1)}$ and therefore their contribution to the observed non-linearities and the spectral function $S(\varepsilon)$ is also very small. The reduced effective volume for the diffusive case is depicted in figure 4(*b*). As already mentioned only those electrons which pass the orifice and then are scattered back inelastically through the orifice (or those electrons which would have passed the contact without the inelastic scattering) contribute to the spectral function $S(\varepsilon)$. Because of the diffusive electron transport with elastic scattering the efficiency of the

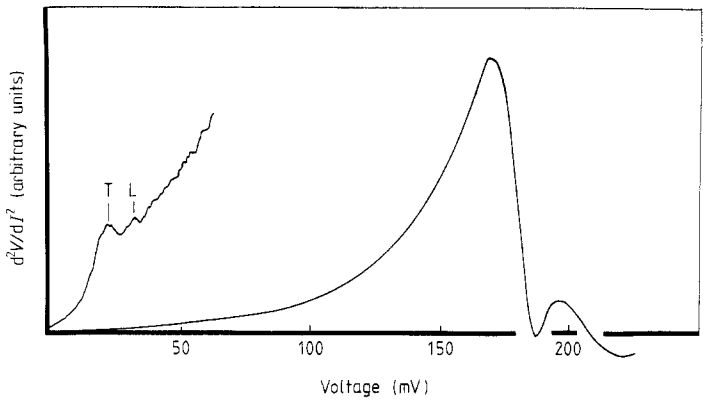

Figure 5. Measured d^2V/dI^2 spectrum of a Ni–Ni point contact with resistance $R_0 = 6.5\ \Omega$ at temperature $T = 1.5$ K, revealing the phonon structure at low voltages (expanded curve) and the ferromagnetic transition at high voltages.

back-flow processes after an inelastic scattering process will be reduced by a factor a/l_e and will be most effective in a volume at a distance l_e from the contact.

3.3. Thermal regime

If the micro-contact diameter d becomes larger than both the elastic and the inelastic mean free paths of the electrons, then the micro-contact is in the thermal regime. In this regime almost all the energy is dissipated in the contact area, which leads to an increase in temperature at the orifice itself. It can be shown that this maximum temperature T_{max} at the centre of the contact for this Maxwell regime is given by (Holme 1967)

$$T_{max}^2 = T_{bath}^2 + V^2/4L \tag{8}$$

where T_{bath} is the bath temperature and L is the Lorenz number. Since by approximation one can say that the centre of the point contact gives the largest contribution to the Maxwell resistance $R_M = \rho/2a$, one actually measures the temperature-dependent resistivity $\rho(T_{max})$ in measuring the voltage-dependent point-contact resistance $R_M(V)$.

Relation (8) can be observed in the measured d^2V/dI^2 spectrum of a Ni–Ni point contact as shown in figure 5. At low voltages this spectrum exhibits the phonon structure, as can be seen in the expanded inset in this figure. From this we can conclude that for these low voltages the contact is in the ballistic or in the diffusive regime. At higher voltages, however, a huge non-linearity shows up which can be understood in terms of the ferromagnetic transition of Ni. At high voltages the electron mean free path becomes so small that the contact is in the thermal regime. Using equation (8) we can calculate the temperature of the contact at the voltage at which the transition is observed. This temperature agrees very well with the Curie temperature of Ni.

An approximation which is less rough than the proportionality $R_M(V) \propto \rho(T_{max})$ mentioned above is the model of spherical spreading out. In this model both the equipotential and the isothermal surfaces are assumed to be hemispheres around the contact. Using this model one can calculate the correlation between the I–V

characteristic and the temperature-dependent resistivity of the metal. One then finds the relation (Verkin *et al* 1980)

$$I(V) = 2Va \int_0^1 \frac{dx}{\rho(T_{max}(1-x^2)^{1/2})} \tag{9}$$

where T_{max} is again the temperature at the centre of the contact, given by equation (8). This relation can be used to calculate the current–voltage characteristics of point contacts in the thermal regime, using the temperature-dependent resistivity of the studied material.

4. The relation between point-contact spectroscopy and tunnelling

For measuring the function α^2F another powerful method exists using superconducting tunnelling (McMillan and Rowell 1965). With superconducting tunnel junctions the normalised density of states $N(E)/N(0)$ in the superconductor can be obtained directly from the differential conductivity $(dI/dV)_S$ in the superconducting state divided by $(dI/dV)_N$ in the normal state. From the measured many-particle density of states, McMillan and Rowell calculated α^2F using an iterative computer calculation. This method can be utilised for strong-coupling superconducting metals. It is however also possible to see the electron–phonon interaction in tunnelling experiments between normal metals because of the inelastic scattering of tunnelling electrons which opens extra channels for the electrons to tunnel through the barrier. Thus in tunnelling experiments with normal metals the inelastic scattering of electrons leads to an increase of the total current. This is the main difference with point-contact spectroscopy, where according to equation (2) the inelastic scattering of electrons gives a negative contribution to the total current (back-flow). As a typical example of the relation between tunnelling and point-contact spectroscopy, we want to mention the experiments on metals with paramagnetic impurities dissolved in them. The experimental results are shown in figure 6. As we will explain in the next section, point-contact experiments on noble metals (e.g. Au or Cu) with paramagnetic impurities (e.g. Mn) show an anomalous structure around zero bias voltage. The observed maximum in the point-contact resistance can be explained in terms of the Kondo problem. Applying an external magnetic field, this maximum is reduced because spin-flip processes are forbidden for voltages $V < g\mu_B B/e$, leading to a structure with a double peak. The decrease of point-contact resistance at zero bias, when applying a magnetic field, can clearly be seen in figure 6(*a*). Figure 6(*b*) shows the results of measurements on a Ta–I–Al tunnel junction (Shen and Rowell 1968). A comparison of both figures clearly shows the opposite behaviour between tunnelling and point-contact spectroscopy. While in the point-contact case the differential resistance dV/dI at $V = 0$ is decreased on applying an external field, in the tunnel experiments it is increased as explained above.

5. Point-contact spectroscopy applied to other scattering mechanisms

As we have already mentioned in the preceding sections the point-contact method has been applied most successfully and most intensively to the scattering of electrons with phonons. However, experiments have also been performed on other inelastic scattering

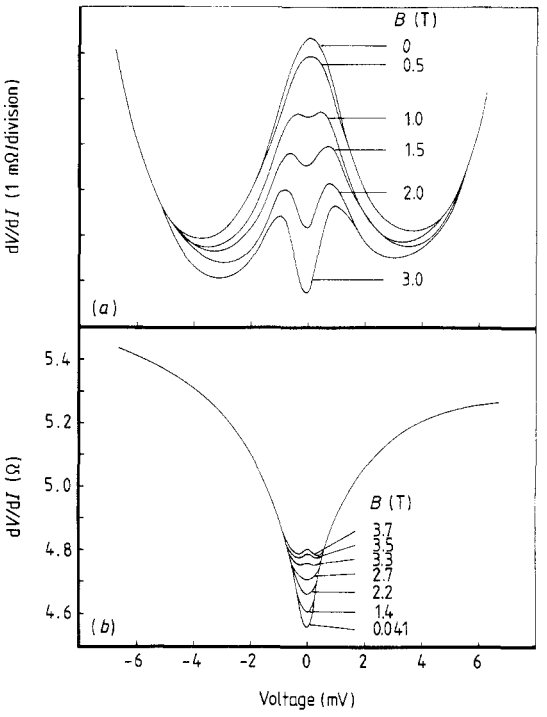

Figure 6. Measured differential resistance dV/dI for (*a*) a Au–0.1 at.% Mn point contact and (*b*) a Ta–I–Al tunnel junction (after Shen and Rowell 1968) at different magnetic fields, showing the opposite behaviour in voltage and magnetic-field dependence between point-contact spectroscopy and tunnelling.

mechanisms. In this section we will discuss briefly a number of point-contact experiments, dealing with scattering mechanisms other than the electron–phonon interaction.

5.1. Electron–magnon scattering

The inelastic scattering of electrons with magnons has been observed most clearly in point-contact experiments by Akimenko *et al* (1982). They carried out experiments on gadolinium, terbium and holmium. For these materials the total of electron–magnon and electron–phonon interaction functions was measured. The most pronounced magnon spectra they found in their experiments on gadolinium. Here the electron–magnon interaction turns out to be much stronger than the electron–phonon interaction since no structure was found at the expected phonon energies. At low energies, theory predicts the electron–magnon interaction function $S(\varepsilon)$ to be proportional to the applied voltage (Kulik and Shekhter 1980). This is indeed found in the experiments on Gd. The experiments with Tb and Gd show the electron–magnon interaction in the spectra superimposed on the electron–phonon structure.

5.2. Crystal-field levels

In point-contact experiments in $PrNi_5$, the level energies of the Pr^{3+} ion in the crystal electric field of this $PrNi_5$ were determined directly (Akimenko *et al* 1984a). The measured spectra show a number of singularities on a rather large background. Observed maxima in the d^2V/dI^2 curves were clearly identified as the Pr^{3+} transition from the ground state into the excited states. This could be made plausible by comparing the point-contact data with the results of neutron scattering experiments.

Applying an external magnetic field shifts the transitions towards somewhat lower energies and induces additional structure due to a transition that was forbidden in zero field.

Crystal-field excitations were also found in point-contact experiments by Frankowski and Wachter (1982). In their experiments on TmSe they found a maximum in the d^2V/dI^2 characteristic at 5 mV which was ascribed to these excitations.

5.3. Scattering with paramagnetic impurities

The differential resistance of point contacts consisting of noble metals with very dilute paramagnetic impurities dissolved in them shows a maximum at zero bias voltage (Jansen *et al* 1980, Duif *et al* 1987). In these Kondo systems the s–d exchange interaction between the conduction electrons and the local moments yields a logarithmic energy dependence of the inverse scattering time $1/\tau(eV)$. As can easily be seen from equation (4), the measured change in differential resistance ΔR is directly proportional to this inverse scattering time $1/\tau(eV)$.

The logarithmic divergence of the energy-dependent scattering rate was measured in the voltage dependence of the point-contact resistance. When an external magnetic field B is applied, the observed zero-bias maximum splits up. This splitting is visible in figure 6. As already mentioned, the decrease in differential resistance and the occurrence of a double peak structure can be explained with the absence of spin-flip scattering at low enough voltages. This type of scattering requires an energy $\Delta = g\mu_B B$, which is not available at low bias voltages. At voltages $V = \pm\Delta/e$, this spin-flip scattering starts contributing again to the differential resistance, yielding a maximum in the contact resistance near these voltages. Using the Hamiltonian for the s–d interaction between conduction electrons and local moments, it is possible to calculate the differential resistance of the point contacts of these systems (d'Ambrumenil and White 1982). From a comparison between measured and calculated spectra the Zeeman energy Δ can be determined as a function of field. Extrapolating this energy Δ to zero external field still leaves in many cases some non-zero value. This can be explained by the presence of internal fields which occur in the somewhat more concentrated samples (spin glasses). These internal fields arise from the indirect exchange interaction (RKKY) between the impurity spins themselves. Figure 7 shows how these internal fields manifest themselves in the measured point-contact spectra. Figure 7(*a*) shows the measured differential resistance of three AuMn point contacts without a magnetic field. In the more concentrated samples a splitting occurs due to the internal fields which become more pronounced when the impurity concentration is increased. Figure 7(*b*) gives the calculated differential resistance for these three samples. A comparison between both plots shows that the theory gives a good description of the experiment.

5.4. Mixed valencies and heavy fermions

In the past few years a considerable number of point-contact experiments have been performed on various valence-fluctuation and heavy-fermion systems. In general, very large non-linearities are found in the current–voltage characteristics, leading to rather large changes in the measured differential resistance dV/dI. In the experiments on valence-fluctuation compounds, both minima and maxima were observed in the resistance around zero bias voltage. For instance, in experiments on YbCuAl and $YbCu_2Si_2$ a minimum was observed in dV/dI (Bussian *et al* 1982). The temperature-

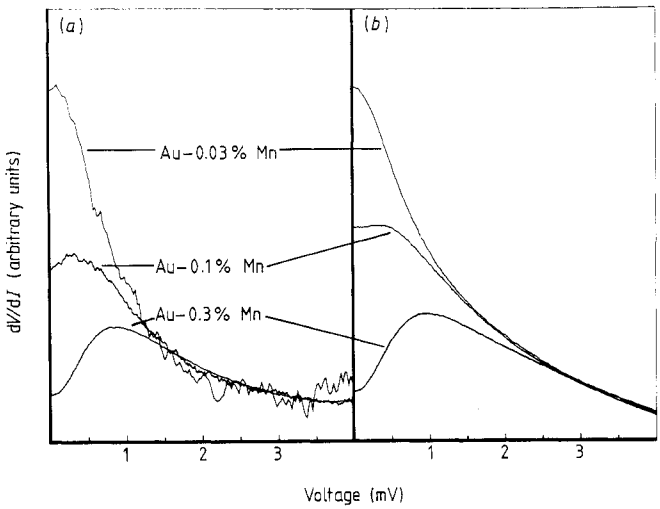

Figure 7. (*a*) Measured differential resistance dV/dI for three AuMn point contacts with different Mn concentrations and (*b*) calculated differential resistance for these contacts.

dependent resistivity $\rho(T)$ of these materials also exhibits a minimum at zero temperature. In experiments on SmB_6 and TmSe a maximum was observed in dV/dI at zero bias voltage (Frankowski and Wachter 1982). However, here the resistivity also has a maximum at zero temperature. Some different interpretations exist of the observed phenomena. Bussian *et al* (1982) explained their results by the energy-dependent inter-configurational scattering of conduction electrons. Frankowski and Wachter (1982) explained their results on TmSe and SmB_6 by the existence of a hybridisation gap in the electron density of states in these materials. In point-contact experiments on heavy-fermion compounds a minimum is found in the differential resistance at zero bias voltage (see e.g. Kunii 1987, Paulus and Voss 1985, Moser *et al* 1985, 1986). This behaviour has been explained by the narrow maximum in the electron density of states around the Fermi level of these materials (Moser *et al* 1985).

Analogously to a tunnelling experiment it is often stated for a point-contact experiment in heavy-fermion systems that the differential conductance dI/dV is proportional to the electron density of states $N(eV)$ at an energy eV above the Fermi level. Hence one could directly probe with a point contact the strong resonance in the density of states around the Fermi level in heavy-fermion systems. However, a simple analysis shows that the energy-dependent density of states does not enter the expression for the resistance of a point contact in the clean limit. To calculate the current in the ballistic limit one has to sum the electron velocity over all possible k-states. The sum over k-states results in an energy-dependent density of states, which is cancelled by the electron velocity. Via the same reasoning as for a tunnelling experiment between normal metals (Harrison 1961), the resistance of a point contact does not contain the energy-dependent density of states in its voltage dependence. For superconductors, however, it is possible to determine the normalised density of states of the superconductor in a tunnelling experiment.

A different approach to the interpretation of the point-contact experiments on these valence-fluctuation and heavy-fermion systems is in terms of the heating model (§ 3.3). It is believed more and more that for the compounds discussed a ballistic point-contact model is not applicable (see e.g. Naidyuk *et al* 1985a).

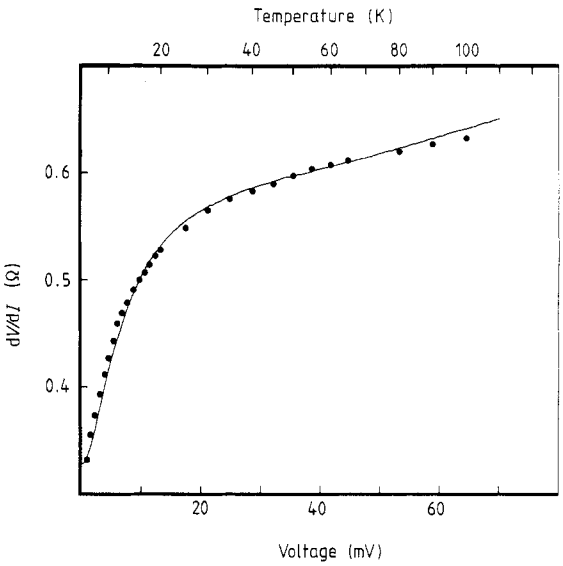

Figure 8. Comparison between the voltage-dependent differential resistance $dV/dI(V)$ of a UPt_3–UPt_3 point contact, measured at 4.2 K (full curve) with its temperature-dependent differential resistance $dV/dI(T)$, measured at $V = 0$ (full circles). Equation (8) has been used for the matching between voltage and temperature scales.

Measurements on UPt_3 (Lysykh *et al* 1988b) show that there is a strong resemblance between the voltage-dependent differential point-contact resistance and the temperature-dependent bulk resistivity of this heavy-fermion system. However, quantitatively the relative change in this temperature-dependent bulk resistivity is a few times larger than the relative change in the voltage-dependent differential resistance. A better quantitative agreement is found by comparing the voltage-dependent resistance at low temperatures with the temperature-dependent resistance at zero voltage. For a normal metal like Cu with point contacts in the clean limit a distinct difference is seen in these two dependences of the point-contact resistance (Jansen *et al* 1988). Still quantitatively the temperature-dependent resistance cannot be explained fully from the temperature-dependent resistivity in terms of the heating model ($R(T) = \rho(T)/2a$). An explanation could be a deviation of the resistivity on the local scale of the point contact compared with the bulk value. Figure 8 shows the comparison between the measured voltage dependence of the differential resistance of a UPt_3–UPt_3 point contact at constant bath temperature (full curve) with the measured temperature dependence of dV/dI at zero bias (full circles). For the scaling between temperature and voltage, equation (8) has been used with experimental values for the temperature-dependent Lorenz number of UPt_3. There is a good agreement between the functional dependence of $(dV/dI)_{V,T=0}$ and $(dV/dI)_{T,V=0}$.

6. Temperature effects in point contacts

In this section we will focus on the thermal aspects of point-contact spectroscopy. It is evident that, in all experiments on point contacts, temperature plays a significant role in the interpretation of the results. As we already mentioned in § 3.3, temperature is essential in the interpretation of the observed current–voltage characteristics of dirty contacts, where Joule heating takes place close to the centre of the contact. For clean contacts the bath temperature determines the resolution of the measured spectra. In equations (2)–(6), for simplicity an infinitesimal temperature ($T \rightarrow 0$) was assumed. At finite tem-

peratures, the measured d^2I/dV^2 spectra will be smeared with a bell-shaped function with half-width $5.4k_BT$ (van Gelder *et al* 1980). It is clear that at helium temperatures this thermal smearing in general does not have a great influence on the spectra since the resolution then is about 1 meV while the spectra in general are much broader than this. Only at higher temperatures does the effect become noticeable.

Recently a number of experiments have been performed in which the transport properties of point contacts were studied with an applied temperature gradient in the contact area. Concerning the heat flux through a contact it was shown that for contacts in the clean limit the quotient of the electrical and thermal resistance follows the Wiedemann–Franz law as for bulk material.

In the presence of electrical and thermal gradients, the influence of thermo-electric effects has been observed in point contacts. In a point contact the phonon-drag contribution to the thermo-power is quenched owing to the small dimensions of the contact. The thermo-power of a point contact therefore shows a difference from that of bulk material.

Point contacts between different materials often show asymmetries in the current–voltage characteristics, which are not expected on the basis of the transport properties of a point contact discussed in § 3. These asymmetries could be due to the Seebeck effect for the case of dirty contacts where the local heating causes intrinsic temperature gradients in the contact.

The measured temperature of the two banks forming a point contact was found to be asymmetric as a function of applied bias voltage. The voltage dependence of these asymmetries reveals phonon structures as can also be measured with normal point-contact techniques.

6.1. Thermal conductivity of metallic point contacts

When a temperature gradient is applied to a point contact, then the transport equations for phonons and electrons again have to be solved using extra boundary conditions which involve the temperature at both sides of the point contact with an applied temperature gradient. In contrast to the thermal conductivity of point contacts between non-conducting systems, in the case of contacts between good conductors, the phonon contribution to the heat flow can be neglected with respect to the electronic contribution. This of course does not mean that the phonon system does not play any role. The scattering of electrons with phonons will influence the current and the heat flow. This, however, will be an effect of second order. In the zeroth-order approximation, comparable with the ballistic injection of electrons without scattering, the heat flux $Q(T)$ can be calculated easily. Measurements of both the thermal and the electrical resistance as a function of temperature enable a determination of the temperature dependence of the Lorenz number $L(T)$, assuming the Wiedemann–Franz law to be valid.

For the electronic distribution (figure 1(*a*)) in zeroth-order approximation, i.e. the pure ballistic case without scattering, the entropy flux I_S is given by

$$I_S^{(0)} = -\frac{ma^2}{2\pi\hbar^3}\int_0^\infty \varepsilon[g^{T_2}(\varepsilon - eV/2 - \mu_2) - g^{T_1}(\varepsilon + eV/2 - \mu_1)]\,d\varepsilon \tag{10}$$

where a quadratic dispersion law is assumed (Bogachek *et al* 1985b). Here the function $g(\varepsilon)$ is given by

$$g(\varepsilon) = f_0(\varepsilon)\ln(f_0(\varepsilon)) + f_0(-\varepsilon)\ln(f_0(-\varepsilon))$$

in which $f_0(\varepsilon)$ is the normal Fermi distribution function. In equation (10) μ_1 and μ_2

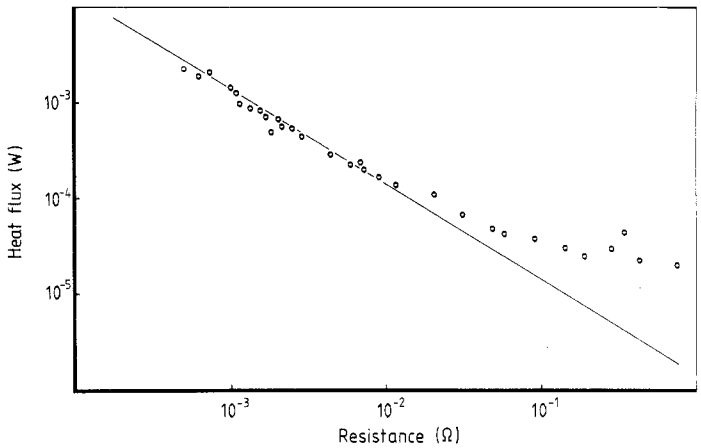

Figure 9. Measured heat flux through different Au–Au point contacts as a function of contact resistance. The temperature at both sides of the contacts was $T_1 = 4.2$ K and $T_2 = 10$ K. The full line represents the theoretical dependence, calculated with equation (12). (After Shklyarevskii *et al* (1986b).)

are the chemical potentials on both sides of the contact at temperatures T_1 and T_2 respectively. From this one can write as a simple result for the entropy flux

$$I_S^{(0)} = -(em/\hbar^3)(\pi a^2/12)(T_1 + T_2)V^* + (\pi^2 k_B^2/3e^2)(T_2 - T_1)/R_{el}. \tag{11}$$

Here $V^* = V + (\mu_1 - \mu_2)/e$ and R_{el} is the electrical resistance of the point contact, given by the Sharvin resistance R_S. Since the first term of this equation is much smaller than the second term, one can write for the heat flux $Q = I_S T$:

$$Q = (\pi^2 k_B^2/3e^2)\, T\Delta T/R_{el}. \tag{12}$$

When $T_2 \gg T_1$ this gives a quadratic temperature dependence of the heat flow. From equation (12) we now find an expression for the ratio between the electrical resistance R_{el} and the thermal resistance $R_{th} = \Delta T/Q$:

$$R_{el}/R_{th} = (\pi^2 k_B^2/3e^2)\, T = L_0 T \tag{13}$$

where L_0 is the Lorenz number. Thus also in the case of point contacts, the Wiedemann–Franz law is valid.

Measurements of the heat flow through metallic constrictions were performed by Shklyarevskii *et al* (1986b). They measured the heat flux through Au–Au point contacts at temperatures between 4.2 and 140 K. Figure 9 shows the measured heat flux Q as a function of point-contact resistance for different contacts. The full line in this figure is calculated with equation (12). A clear agreement is found between theory and experiment for contact resistances below approximately 0.01 Ω. For contacts with a larger resistance there is a strong discrepancy between theory and experiment. It can be assumed that in these cases the phonon flow through electrically non-conducting regions of the contact is large compared with the heat flow by electrons through the contact. For low contact resistances the measured heat flux is indeed quadratic in temperature up to 20–30 K, according to equation (12) for large $\Delta T = T - 4.2$ K. At higher temperatures the exponent in this dependence is slightly smaller and for very low resistances (i.e. large contact diameter) it even becomes linear, which is in agreement with the constant thermal conductivity for bulk metals at sufficiently high temperatures.

Equation (13) provides a possibility of measuring the temperature dependence of the Lorenz number L. In the cited experimental work, the temperature dependences of L was determined. The behaviour found is similar to that for bulk metal.

6.2. Thermo-electric effects in metallic point contacts

Recently a number of experiments have been performed which studied the influence of the presence of a temperature gradient in the contact region on the electrical properties of both metallic and semiconducting point contacts. In this section we will discuss the case of metallic contacts, and in the next section look at semiconducting ones. Temperature gradients in the contact region can be obtained by heating one side of the contact, but also by Joule heating by a current through the contact.

In the case of a homogeneous contact with a temperature difference $\Delta T = T_2 - T_1$ across it, the electrical current for a ballistic contact is given by

$$I^{(0)} = \frac{ema^2}{2\pi\hbar^3} \int_0^\infty \varepsilon[f_0^{T_2}(\varepsilon - eV/2 - \mu_2) - f_0^{T_1}(\varepsilon + eV/2 - \mu_1)]\,\mathrm{d}\varepsilon \qquad (14)$$

where f_0^T is the Fermi distribution at temperature T, and μ_1 and μ_2 are the temperature-dependent chemical potentials. Usually, i.e. when no temperature gradient is applied, this equation leads to the Sharvin resistance. With an applied temperature gradient it is possible to calculate from equation (14) at zero current density the diffusion term $S_{\mathrm{pc}}^{\mathrm{e}}$ in the thermo-power of the point contact, which is then given by

$$S_{\mathrm{pc}}^{\mathrm{e}} \equiv \lim_{\Delta T \to 0} \frac{\Delta\mu - eV}{e\Delta T}\bigg|_{I=0} = -\frac{1}{eT}\left(\frac{F_2}{F_1} - \mu_1\right) = -\frac{\pi^2 k_{\mathrm{B}}^2 T}{3e\mu_1}. \qquad (15)$$

Here $\Delta\mu = \mu_2 - \mu_1$ is the difference in chemical potential, and F_1 and F_2 are given by

$$F_{\mathrm{n}} = \int \varepsilon^n (\partial f_0/\partial\varepsilon)\,\mathrm{d}\varepsilon.$$

Here a free-electron model with a spherical Fermi surface was assumed. The diffusion term $S_{\mathrm{pc}}^{\mathrm{e}}$ is linear in temperature. For a bulk material a similar expression is found in a simple model with a constant mean free path (Barnard 1972). We want to emphasise the fact that this is only the electron-diffusion term in the thermo-power. In a metal the total thermo-power is given by $S = S^{\mathrm{e}} + S^{\mathrm{ph}}$ where S^{ph} is the phonon-drag term in the thermo-power, which is due to the transport of electrons by the non-equilibrium phonon system. The temperature dependence of the phonon-drag thermo-power S^{ph} of bulk metals shows a maximum at about $0.2\theta_{\mathrm{D}}$ where θ_{D} is the Debye temperature. This is because this phonon-drag component in a simple model is proportional to the lattice specific heat with a reduction factor $\alpha = \tau_{\mathrm{p,x}}/(\tau_{\mathrm{p,x}} + \tau_{\mathrm{p,e}})$ for the efficiency of energy transport from the phonon system with respect to the electrons ($\tau_{\mathrm{p,e}}$ is the phonon–electron scattering time and $\tau_{\mathrm{p,x}}$ the scattering time of phonons with other scatterers, e.g. phonons). At low temperatures the phonons interact primarily with electrons and $\alpha = 1$, but at high temperatures $\alpha = 0$. As a result the thermo-power of bulk material shows a maximum superimposed on a linear term from the diffusional contribution of the electrons. Note that for the electronic thermo-power S^{e} of bulk metals, the same expression is found as equation (15) for the point-contact case. In the point-contact case, however, at low temperatures, the scattering of phonons ($\tau_{\mathrm{p,x}}$) will be determined by the contact dimension so that α will be small and the phonon drag will be suppressed. Therefore the phonon-drag term of the bulk material will be larger than that of a point contact.

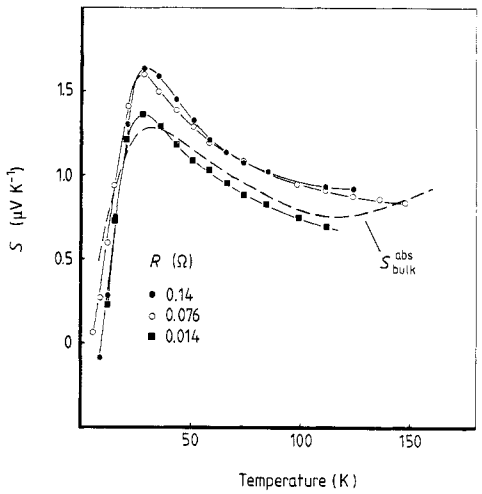

Figure 10. Measured thermo-power $S = S_{bulk} - S_{pc}$ as a function of temperature, measured over Au chains containing point contacts with indicated resistances. The broken curve represents the absolute thermo-power S^{abs}_{bulk} for Au. (After Pearson (1961).)

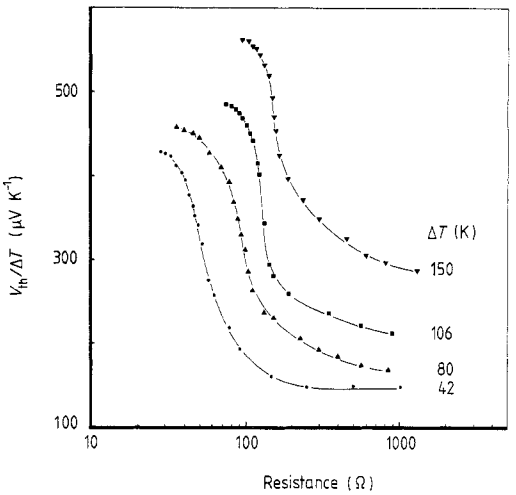

Figure 11. Thermo-electric voltage V_{th}, divided by the temperature difference ΔT, measured over Cu–Si–Cu chains with a constriction in the Si, as a function of contact resistance for different applied temperature gradients WT over the contact as indicated in the figure. One side of the contacts was always kept at a constant temperature $T_1 = 300$ K. (after Trzcinski *et al* (1986).)

Thermo-powers in homogeneous metallic point contacts were measured by Shklyarevskii *et al* (1986a). In their experiment, the Seebeck voltage was measured between the isothermal terminals of a chain, made of one metal and containing a point contact, over which a temperature difference $\Delta T = T - 4.2$ K was applied by heating one side of the contact. The measurements were performed without any electrical current. The measured Seebeck voltage in this case is equal to the difference between the thermal voltage over the bulk part and the point-contact part such that

$$V_{tot}(T) = V_{bulk} - V_{pc} = \int_{4.2}^{T} [S_{bulk}(T') - S_{pc}(T')]\,\mathrm{d}T'. \tag{16}$$

Here S_{bulk} and S_{pc} are the bulk and the point-contact thermo-powers. An example is given in figure 10 for a Au point contact. We see that the measured thermo-power $S = S_{bulk} - S_{pc}$ resembles (even in absolute value) the bulk thermo-power which is also plotted in this figure. In view of the comparison discussed before, between the thermo-power of bulk material and a point contact, one expects to measure mainly the term S^{ph}_{bulk} in the set-up with the metallic constriction. At low temperatures there is a difference in the measured thermo-power for different point contacts measured in the same set-up. Probably these effects are due to the Kondo effect, because especially the thermo-power is very sensitive to small amounts of paramagnetic impurities. Because of a local distribution of paramagnetic impurities the measured thermo-power changes from contact to contact with respect to the bulk thermo-power. In measurements on Ag these effects were absent and the bulk thermo-power was directly obtained in the point-contact arrangement. At high temperatures the measured thermo-power becomes constant. This constant background is not yet explained.

Another case in which thermo-electric effects come into play is that of a current flowing through a non-homogeneous point contact in the thermal limit. When heating occurs in the contact region, then the Seebeck effect will cause an extra voltage over the contact due to the different thermo-powers of the two materials that form the contact. Besides this effect the Peltier effect will cause an extra heating or cooling of the contact, depending on the direction of the current flow. A third effect, the Thomson effect, gives an extra heating in the contact area due to the presence of both a temperature gradient and an electric field. All these three effects together influence the voltage over the contact and consequently asymmetries in the current–voltage characteristics and their derivatives are observed. At low temperatures (i.e. low voltage over the dirty contact) the Seebeck effect is dominant.

These thermal voltages and asymmetries of the current–voltage characteristics in non-homogeneous point contacts were studied by Naidyuk *et al* (1985b). The most pronounced example that they found of the studied phenomenon was the shift in voltage at which the ferromagnetic transition shows up in Cu–Ni point contacts. As we already showed in figure 5, point contacts consisting of Ni show this transition around 190 mV, which corresponds in view of the heating model (equation (8)) with the Curie temperature of Ni. In experiments on Cu–Ni the same transition occurs, but now however it also depends a little on the sign of the applied bias. The difference ΔV between positive and negative bias is approximately 10 mV. This asymmetry can be explained by the Seebeck effect. Analogous to equation (16) one can easily show that the observed difference $\Delta V(V)$ must be equal to

$$\Delta V(V) = 2\int_{T_{\text{bath}}}^{T_{\max}} [S_{\text{A}}(T) - S_{\text{B}}(T)]\,\mathrm{d}T \tag{17}$$

in which T_{bath} is the bath temperature, $T_{\max}$ is the maximum temperature at the centre of the contact given by equation (8), and $S_{\text{A}}(T)$ and $S_{\text{B}}(T)$ are the temperature-dependent thermo-powers of materials A and B between which the point contact is made. Calculation of this integral, using the temperature-dependent thermo-powers of Ni and Cu as known from literature, gives $\Delta V \simeq 22$ mV, which is of the same order as the measured value. This only gives a crude estimate of the voltage difference ΔV since at these high temperatures also the Peltier and Thomson effects have to be incorporated.

Finally measurements were performed on Cu–CuFe and Cu–CuMn point contacts. Here already an asymmetry is observed for low energies ($eV \ll k_{\text{B}}\theta_{\text{D}}$) in the structure related to the Kondo effect. These contacts are believed to be in an intermediate state between diffusion and ballistic regimes. From the observed asymmetry it can be concluded that even in this case a non-uniform temperature distribution is present in the contact area. It is possible that this temperature distribution has to be seen as the non-equilibrium distributions of electrons and/or phonons on both sides of the contacts.

6.3. Thermo-electric effects in semiconductor point contacts

Up to the present, electrical measurements on semiconductor point contacts have only been performed in short-circuited metal–oxide–semiconductor (MOS) structures (Pepper 1980a, b, c), showing a rich structure in the spectra due to phonons, and in In–InGaAs microchannel contacts, where an oscillatory behaviour is found due to LO phonons (Pong-Fei Lu *et al* 1985). A problem in pressure-type contacts with semiconductors is the very large contact resistance which occurs in most cases. Most probably surface states play a dominant role in this kind of experiment, leading to

irreproducible results. In metal–semiconductor point contacts a Schottky barrier will be formed, thus leading to large contact resistances at low voltages and large non-linearities.

With a Cu–semiconductor–Cu chain with a constriction in the semiconductor part, Trzcinski *et al* (1986) measured the thermo-electric voltage of Si point contacts as a function of contact resistance. No electrical current was applied but one side of the contact was heated. Thus this experiment is the semiconductor equivalent of the experiment by Shklyarevskii *et al* (1968a) on metals, as discussed in § 6.2, but here the experiments were performed at room temperature. Also here the thermo-power can be thought to exist of an electronic part and a phonon-drag part. Figure 11 shows the measured thermal voltage over the contacts, measured as a function of contact resistance for different applied temperature gradients. At a certain resistance, slightly dependent on the applied temperature gradient, a sharp drop in thermal voltage takes place within a narrow range of R. This sudden drop is ascribed to the quenching of phonon drag when the phonon mean free path becomes comparable with the contact dimension. The observed temperature dependence can be explained by the presence of more short-wavelength phonons at higher temperatures for which the scattering is less affected by a size reduction and therefore the effect occurs at smaller contact dimensions. A universal scaling was found, combining the effects of temperature and sample dimension.

6.4. Thermal phonon spectroscopy in Cu point contacts

In § 6.1 we already discussed heat transport through metallic contacts due to an applied voltage and a temperature difference between the contact members. However, the discussed transport is only the zeroth-order approximation, comparable with the zeroth-order solution in the electrical case, i.e. the ballistic injection of electrons without any scattering. In both cases no electron–phonon scattering effects can be expected to show up in the observed characteristics. In the second-order solution, however, these effects have to be considered. Bogachek *et al* (1985b) predicted a voltage-dependent first-order heat flux $Q^{(1)}$, from which the second derivative is given by

$$\frac{d^2Q^{(1)}}{dV^2} = -\tfrac{8}{3}\pi e^3 a^3 A N(0) V \alpha^2 F_p(T, eV/\hbar) \tag{18}$$

where A is a factor that is a measure of the regime in which the contact is. For instance, in the ballistic regime this constant A is equal to unity. In the thermal regime, however, it is reduced to $A = 8l_e/3\pi a \ll 1$. This means, as we have already seen in the electric spectra, i.e. d^2V/dI^2, that the signals are considerably reduced when the contact is not (any more) in the ballistic state. In equation (18) $N(0)$ is the electron density of states at the Fermi surface and the temperature dependence of the function α^2F_p has to be taken into account. We must remark that this equation (18) is only valid for the case in which there is no temperature difference between both parts of the contact, i.e. $T_1 = T_2$. For the case where the parts of the contact are not strictly kept at the same temperature, a temperature difference will occur which will also contain structure because of the electron–phonon interaction.

Experiments on this subject were reported by Reiffers *et al* (1986). They measured very accurately the temperature of both the two contact members as a function of the applied voltage. Their contacts were made between two pieces of bulk material to which

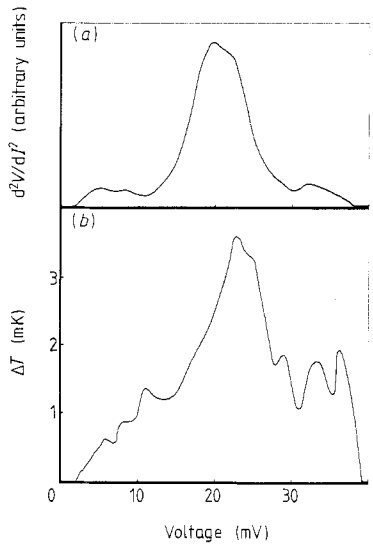

Figure 12. Comparison between (*a*) the measured d^2V/dI^2 spectrum as a function of bias voltage of a Cu point contact with resistance $R_0 = 0.84\ \Omega$ at temperature $T = 0.72$ K and (*b*) the measured asymmetry ΔT in temperature difference between the two contact members, between positive and negative bias for the same contact at the same bath temperature. (After Reiffers *et al* (1986).)

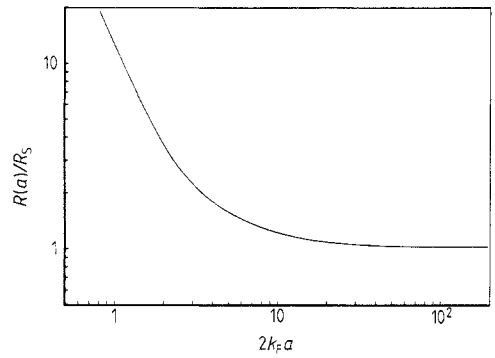

Figure 13. Calculated contact resistance $R(a)$, normalised with the Sharvin resistance R_S, plotted as a function of k_Fa, showing the quantum-mechanical deviations from this Sharvin resistance for contacts with very small diameters.

thermometers were attached. In the measurements of temperature versus applied bias voltage, an asymmetry was found with respect to $V = 0$. In figure 12 their results are depicted. Figure 12(*a*) gives the well known electron–phonon interaction point-contact spectrum of copper, whereas figure 12(*b*) gives the measured temperature difference between positive and negative bias as was measured in these experiments. There is a striking resemblance between the measured second derivative d^2V/dI^2 and the measured temperature difference ΔT in this experiment. The occurrence of maxima at the same energies at which the phonon peaks in d^2V/dI^2 occur implies that the electron–phonon interaction in this experiment also plays an essential role in the shape of the measured asymmetry, as was more or less predicted by the theory of Bogachek *et al* (1985b).

Besides the broad maxima at the energies of the transverse and longitudinal phonons, additional structure with maxima and minima is found in these experiments, which probably occur due to different mechanisms of scattering. The positions of these maxima and minima are in reasonably good agreement with the positions of the extrema in noise spectra of copper point contacts (Akimenko *et al* 1984b).

7. Special experiments on and with point contacts

We will now discuss a number of experiments that have been performed recently and are different from the traditional type of experiment, in which interaction mechanisms of the conduction electrons with elementary excitations in the metal are studied.

The influence of a magnetic field for instance on bulk material is fairly well understood but a point contact shows some unexpected and interesting features when it is placed in a magnetic field. Measurements on point contacts in high magnetic fields display a quadratic magneto-resistance on which are superimposed Shubnikov–de Haas like oscillations.

Metallic point contacts can also be brought into a high-frequency (HF) electromagnetic field. Already for some time they have been used as HF rectifiers, mixers and harmonic generators. The origin of the rectifying mechanism can be explained in terms of the discussed models of the non-linear current–voltage characteristics of point contacts. Also here one has to distinguish between point contacts in the ballistic and those in the thermal regime. The results of measurements in both these regimes are different. This provides a new method to distinguish between the two regimes. When the applied laser frequency is chosen large enough, photon-assisted tunnelling effects come into play.

With double point contacts a number of experiments have been performed in which the electrons were injected by the first contact and with help of a transverse magnetic field were focused onto the second contact. This set-up gives the possibility to study the Fermi surface of the metal and even the energy dependence of the electron–phonon interaction for electrons in a specific orbit on the Fermi sphere.

Noise measurements on Cu–Cu show that point contacts exhibit a $1/f$ noise spectrum. As a function of applied bias voltage the spectral density of this noise shows a quadratic dependence. However, on this quadratic dependence a structure with minima and maxima is superimposed. The positions of these extrema coincide with different phonon processes in the examined material.

Finally experiments are described in which the phonon spectrum generated with a point contact was examined. In the ballistic regime one expects a phonon distribution with a cut-off energy equal to the applied energy eV. In an experiment in which B^+ impurities in Si were used as a phonon detector, this distribution could not be confirmed, probably due to a premature thermalisation of the phonon system.

7.1. Point contacts in high magnetic fields

Magnetic fields have mostly been applied in point-contact experiments as a tool to change some material parameters of the metal under study. For instance, magnetic fields have been used to quench superconductivity in order to enable measurements of the electron–phonon interaction for point contacts in the normal state. Another example is the influence of magnetic fields on magnetic excitations to be studied with the point-contact technique. However, recently also a number of experiments have been performed in which the direct influence was studied of a magnetic field on the point-contact resistance. The most striking phenomena that occur in these experiments are the observed magneto-resistance and an oscillating magnetic-field dependence of the contact resistance.

Owing to the change in the electron trajectories, the magnetic field affects the resistivity of the material under study. For a sufficiently large transverse magneto-resistance, the resistance of a contact has an additional term given by the square resistance ρ/d of the sample (thickness d) on which the point contact is put. Hence the point-contact resistance changes as the bulk magneto-resistivity. The superimposed oscillatory behaviour of point contacts in magnetic fields can be ascribed to the Landau quantisation of the electron orbits.

7.1.1. Magneto-resistance in metallic point contacts. We will first focus on the observed classical magneto-resistance in metallic point contacts. As we already mentioned in § 2, in a simple picture the point-contact resistance can be thought to exist of a ballistic part, the Sharvin resistance, and a diffusive part, the Maxwell resistance (equation (1)). For a clean contact the Sharvin resistance will dominate and the Maxwell resistance will hardly be noticeable. However, the resistivity of the material under study changes considerably on applying a magnetic field. The resistivity-dependent component of the contact resistance becomes more important, and can even give the main contribution to the observed magneto-resistance.

The resistivity of a metal in general depends strongly on the direction and size of the magnetic field. We must however distinguish here compensated metals, i.e. where the number of holes and electrons is equal, and uncompensated metals. In the case of compensated metals the transverse magneto-resistivity ρ_t is according to the LAK theory (Lifshitz *et al* 1956) given by

$$\rho_t = (1 + \beta^2)\rho_0. \tag{19}$$

Here ρ_0 is the zero-field resistivity and β is a parameter proportional to the magnetic field which in a simple picture equals $\beta = \omega_c\tau$, with the cyclotron frequency $\omega_c = eB/m^*$, and the electron relaxation time τ. The longitudinal resistivity ρ_l is not affected by the magnetic field. In high magnetic fields, values for β of 10^3 can easily be obtained for pure materials and the resistivity will be very anisotropic in a magnetic field. As a consequence the point-contact resistance will have an important component originating from the resistivity perpendicular to the magnetic field. For a point contact placed on a sample of thickness d in a magnetic field perpendicular to this sample, the magneto-resistance component resembles the square resistance ρ_t/d and the modified expression for the Maxwell resistance can be written as

$$R = (1 + \beta^2)(\rho/2\pi d)\ln(D/4a). \tag{20}$$

Here D is the sample diameter, where the sample is assumed to be circular with the current and voltage contacts on its border, and a is the radius of the point contact. From equation (20) we see that we can also expect a quadratic magnetic-field dependence of the contact resistance as in bulk materials. With the semi-classical theory no effect of a magnetic field is expected on the Sharvin resistance, which is independent of the electronic scattering time.

In an experiment Swartjes and co-workers measured this effect on bismuth (Swartjes *et al* 1988a). They measured both the bulk and the point-contact magneto-resistance of this material. A comparison of both measurements confirmed the validity of equation (20) for the resistance of a point contact in a magnetic field.

In the case of uncompensated materials, the magneto-resistance is usually very small. However, in the Corbino geometry with a central contact on a circular sample, and the other contact on the total contour, again a quadratic magnetic field dependence is found. The origin for this magneto-resistance lies in the circular symmetry of the Corbino geometry, which hinders the build-up of a Hall voltage. Usually in uncompensated metals, the Hall voltage compensates the deflection of electrons in a magnetic field, and the magneto-resistance is small. A point contact can be regarded as a Corbino geometry and will thus exhibit a considerable magnetic-field dependence. In this case a similar expression to equation (20) can be given for the point-contact magneto-resistance. In a point-contact experiment with Al this effect was observed (Swartjes *et al* 1988a).

7.1.2. Magneto-oscillations in metallic point contacts. It is commonly known that a number of physical quantities of metals show oscillations when measured as a function of magnetic field. The origin of these oscillations lies in a redistribution of the electrons when the Landau tubes cross the Fermi surface for increasing magnetic field. Well known examples of this oscillatory behaviour are the de Haas–van Alphen effect in the magnetic susceptibility and the Shubnikov–de Haas effect in the electrical resistivity. The latter manifests itself in the modified expression for the Maxwell resistance since according to equation (20) this is proportional to the resistivity. However, also the Sharvin term in the point-contact resistance can show oscillations in the magnetic-field dependence because of diffraction of the electronic wavefunctions at the orifice.

When the typical length on which an electron is localised becomes large compared with the contact dimension, a semi-classical calculation as is used to derive the Sharvin resistance is not applicable any more, but a quantum-mechanical approach is necessary. In the case of no applied magnetic field, this length is the de Broglie wavelength $\lambda = 2\pi/k_F$ which will in most cases be small compared with the contact dimension. When a magnetic field is applied, this length becomes the magnetic length $\Lambda = (2\hbar/eB)^{1/2}$ which is comparable with the contact dimension for fields of the order of 5 T.

A quantum-mechanical approach with the Wigner formalism for the problem was used by Bogachek *et al* (1985a) for the case $\Lambda \ll a$. They found oscillations in the point-contact resistance proportional to $z^{-3/2}$, where $z = \mu/\hbar\omega_c$ is the number of filled Landau levels below the chemical potential μ. In another approach (Swartjes *et al* 1988b) the problem is considered as a diffraction problem for the case $\lambda > a$ or $\Lambda > a$. The wavefunctions of the incoming electrons will lose their directional information after passing the contact. As a consequence of this, in the derivation of the Sharvin resistance, which is a summation over all the perpendicular components of the electron velocity in k-space, i.e. $\int d^3k\, v_z$, the term $dk_z\, v_z$ has to be replaced by $\Sigma_{j'} dk_{z,j}\, v_{z,j'} \Delta_\gamma(j, j')$, where the summation goes over all possible plane-wave directions of the outgoing electron. The function $\Delta_\gamma(j, j')$ describes the coupling between k_z and v_z and depends on the ratio γ between contact diameter and electron wavelength. A calculation using this approach, for the case that no magnetic field is applied, yields (Swartjes *et al* 1988b)

$$\frac{1}{R} = -\frac{e^2}{2\pi\hbar}\frac{Sk_F^2}{2\pi}\int_0^{2k_Fa} d\xi\, \eta\left(\frac{\xi}{2k_Fa}\right)\frac{d}{d\xi}\left(\frac{\sin\xi}{\xi}\right)^2 \tag{21}$$

which in the semi-classical limit $k_Fa \gg 1$ reduces to the Sharvin resistance R_S. In this equation S is the contact area and $\eta(\xi)$ is the overlap of the contact with itself when shifted over the vector ξ. This ξ is any vector lying in the contact area. Equation (21) describes the quantum-mechanical deviation from the Sharvin resistance R_S for contacts with a dimension comparable with the inter-atomic distance. In figure 13 the resistance calculated with equation (21), normalised with the Sharvin resistance, is plotted as a function of k_Fa for circular contacts with radius a. Note that for large k_Fa the point-contact resistance equals the Sharvin resistance and hence the problem can be treated semi-classically.

When a magnetic field is applied, the summation in the calculation of the Sharvin resistance now goes over wavefunctions of electrons in a magnetic field, instead of over plane waves, and the index j' now goes over all Landau levels. A calculation (Swartjes *et al* 1988b) yields two separate oscillations in the point-contact resistance, one with relative amplitude $z^{-3/2}$ and one with $z^{-1/2}$. Including the diffraction at the orifice of an electron wavefunction in a magnetic field, a considerable enhancement

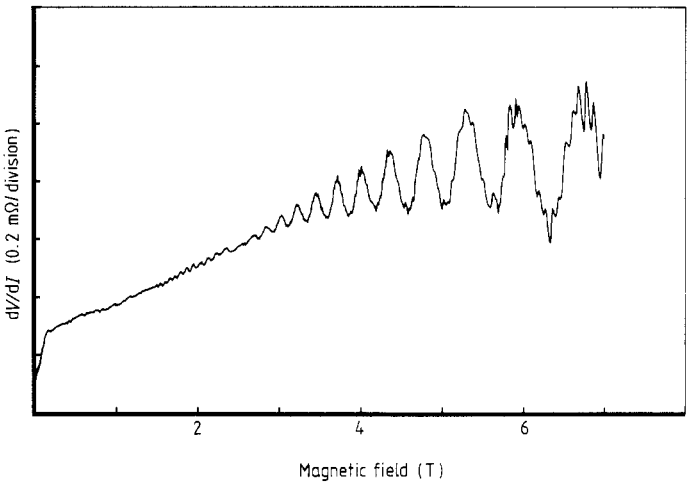

Figure 14. Measured differential resistance dV/dI of an Al–Cu point contact with resistance $R_0 = 1.3\,\Omega$ at temperature $T = 1.85$ K, as a function of magnetic field, showing the magneto-oscillations of point contacts in magnetic fields.

is expected of the oscillatory quantum effects in the magneto-resistance of a point contact ($z^{-1/2}$ dependence compared with $z^{-3/2}$). Figure 14 gives an example of these quantum-mechanical oscillations of a point contact in a magnetic field. The resistance of an Al–Cu point contact shows an oscillatory behaviour, periodic in $1/B$, which can be ascribed to Landau tubes in the third zone of the Fermi surface of Al.

7.2. Point contacts in high-frequency electromagnetic fields

Already for a long time point-contact diodes have been used as rectifiers, mixers and harmonic generation elements for high-frequency purposes, i.e. for frequencies up to the near-visible. The point contacts that are used for these cases consist of a whisker, sharpened to a small point and put on a piece of bulk material. The whisker serves as an antenna through which a high-frequency current is induced inside the contact. Because of the non-linear current–voltage characteristic of such a point contact, the element can be used for purposes as mentioned above.

When a point contact is brought into a high-frequency electromagnetic field, the radiation field acts as a high-frequency current source, because the point-contact resistance is usually smaller than the vacuum impedance. Chopping the radiation at a low frequency, it can easily be shown that the measured voltage at this chopper frequency is proportional to the second derivative d^2V/dI^2 as measured with the traditional techniques, using low-frequency current modulation. Thus with this technique it is for instance also possible to measure the α^2F function, however now using a modulation with a much larger frequency. This effect was first observed by van der Heijden *et al* (1980), who measured this rectification by a Cu–Cu point contact and found a laser-detected signal which was completely in agreement with the measured second derivative d^2V/dI^2, as measured with low-frequency modulation.

In order to measure a signal proportional to the second derivative d^2V/dI^2, the processes that determine the current–voltage characteristics have to be fast compared with the applied HF modulation frequency. In the experiments by van der Heijden *et*

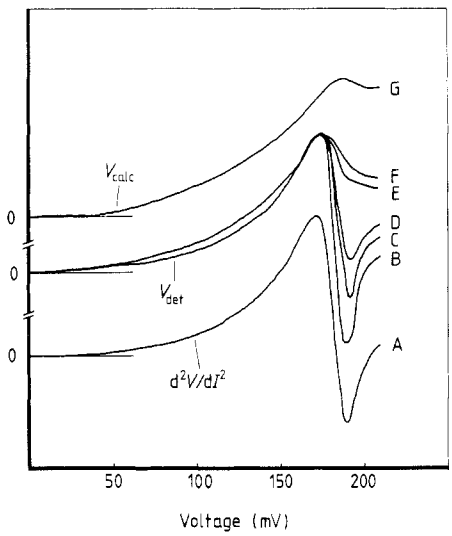

Figure 15. Measured d^2V/dI^2 spectrum (A), rectification signals at five different HF modulation frequencies (B–F) (after Balkashin *et al* 1982) and the calculated rectification signal for the thermal regime (G) as a function of applied voltage for a Ni–Ni point contact with a resistance $R_0 \simeq 3.3\,\Omega$ at room temperature. The curves have been shifted with respect to each other. The applied radiation frequencies were (B) 0.3, (C) 1.0, (D) 2.0, (E) 12 and (F) 16.6 GHz. The theoretical curve was calculated with equation (22).

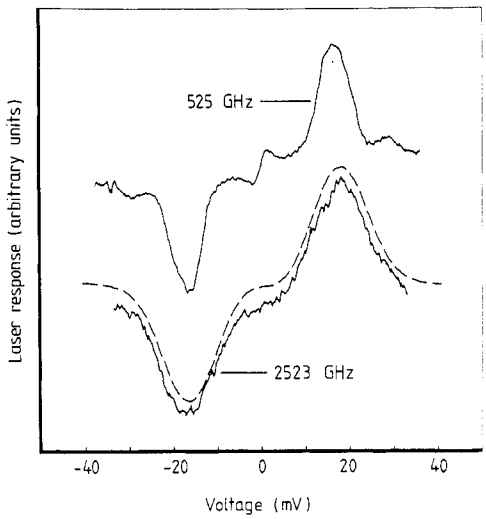

Figure 16. Rectification signals measured with a radiation frequency of $\omega = 525$ GHz for a Cu–Cu point contact with resistance $R_0 = 4.9\,\Omega$ at temperature $T = 1.2$ K (upper full curve) and with radiation frequency of $\omega = 2523$ GHz for a Cu–Cu point contact with resistance $R_0 = 42.1\,\Omega$ at temperature $T = 1.2$ K (lower full curve). In this latter curve the photon-assisted tunnelling effect gives a considerable broadening of the spectrum. The broken curve was calculated with equation (23).

al (1980) the characteristic time τ for these processes is the electron–phonon scattering time $\tau_{\text{el-ph}}$ which is typically 10^{-14}–10^{-13} s for Cu at helium temperatures. Therefore the criterion $\omega_{\text{rad}}\tau < 1$ for the laser-detected signal to follow the non-linear DC current–voltage characteristics is fulfilled in these experiments.

The criterion $\omega_{\text{rad}}\tau < 1$ will not hold any longer in the situation where heating is the main effect that determines the current–voltage characteristics. Then the characteristic time constant τ_{thermal} for the non-linearity is given by the thermal relaxation of the contact. It is given by the quotient of the total heat capacity of the contact and the conduction of heat out of the contact area, i.e. $\tau_{\text{thermal}} \sim C/\Lambda \simeq cd^3/(\lambda d^2/d) = cd^2/\lambda$, where d is the contact diameter, c is the specific heat and λ is the thermal conductivity of the metal under study. For a contact with a typical dimension of $d \sim 10$ nm one finds $\tau_{\text{thermal}} \sim 10^{-9}$ s; hence the signals will change in this regime at frequencies in the gigahertz regime. An example of this is the experiment by Balkashin *et al* (1982), who measured the rectification signal of a Ni–Ni point contact at room temperature for different HF modulation frequencies. Figure 15 gives their results. Curve A gives the measured second derivative d^2V/dI^2 obtained with the standard technique at 483 Hz, showing the ferromagnetic transition due to heating of the contact area (see also figure 5). Curves B–F are the rectification signals measured with increasing frequency. For frequencies below 300 MHz the observed signal resembles the d^2V/dI^2 spectrum. At higher frequencies deviations occur from this behaviour. One can conclude that the

timescale imposed by the 300 MHz radiation is of the same order of magnitude as the thermal relaxation time of the contact. At higher radiation frequencies the temperature cannot follow the modulated current and a constant rise in temperature due to the HF current modulation will occur. It is easily shown that the signal detected in the experiment is given by (Lysykh *et al* 1988a)

$$V_{\text{det}} = (\sqrt{2}i^2/8)\, R_s(\mathrm{d}R_s/\mathrm{d}V) \tag{22}$$

where R_s is the static resistance of the point contact and i is the amplitude of the induced HF current. This theoretical rectification signal is also plotted in figure 15 (curve G). There is a strong resemblance between this curve and the signal measured at the highest frequency (16.6 GHz). Complete agreement is not found since probably the criterion $\omega_{\text{rad}}\tau \gg 1$ is not yet totally fulfilled at this frequency.

Also for the electron–phonon interaction in clean contacts it is possible that the measured rectification signal does not resemble the second derivative $\mathrm{d}^2V/\mathrm{d}I^2$. A considerable broadening of the spectra occurs when the changes in the I–V characteristics take place on a voltage scale comparable with or larger than $\hbar\omega_{\text{rad}}/e$ of the applied radiation. This broadening, only occurring at higher radiation frequencies, can be described with the photon-assisted tunnelling (PAT) theory (Tien and Gordon 1963). The PAT effect can be considered as the quantum-mechanical analogue of classical rectification and is mostly observed in tunnelling experiments with superconductors. In figure 16 the broadening at high radiation frequencies is shown. The upper full curve represents the rectification signal for a Cu point contact measured at a laser frequency of 525 GHz (i.e. 2.2 meV). The shape of the signal resembles the $\mathrm{d}^2V/\mathrm{d}I^2$ spectrum of Cu (see e.g. figure 2). The lower full curve gives the rectification signal of a Cu point contact, measured at a laser frequency of 2523 GHz (i.e. 10.4 meV). Here the broadened signal is fitted with the broken curve, which is calculated using the PAT expression for the DC current at voltage V when radiation is applied:

$$I_{\text{DC}}(V) = \sum_{n=-\infty}^{n=+\infty} J_n^2(\alpha)\, I(V + n\hbar\omega_{\text{rad}}/e) \tag{23}$$

where $I(V)$ is the DC current in the absence of radiation, J_n is the nth-order Bessel function and $\alpha = eV_{\text{AC}}/\hbar\omega_{\text{rad}}$ in which V_{AC} is the induced HF modulation voltage over the contact. Photon-assisted tunnelling is mostly seen in experiments on non-linear elements in which a superconductor is involved. In the experiment by van der Heijden *et al* (1984, figure 16) it was observed for the first time in a normal metal element.

7.3. Transverse electron focusing with double point contacts

Electrons can be focused by a magnetic field in a metal from one point contact to another, revealing details of the trajectories on the Fermi surface. In the experiments the electrons are injected into a single crystal with a point contact (the emitter) and after focusing are detected with a second point contact (the collector). The first experiments of this type were performed by Sharvin and Fisher (1965). They placed emitter and collector at opposite sides of the crystal with the focusing magnetic field parallel to the axis between the two contacts. The method of focusing electrons between two contacts was improved by Tsoi (1974) by using a transverse magnetic field instead of a longitudinal one. The emitter and collector were now placed on the same side of the crystal (see inset of figure 17). This opened up the possibility to study the Fermi-surface orbits and specular reflections of the conduction electrons with the crystal surface. With this method of transverse electron focusing it turned out to be

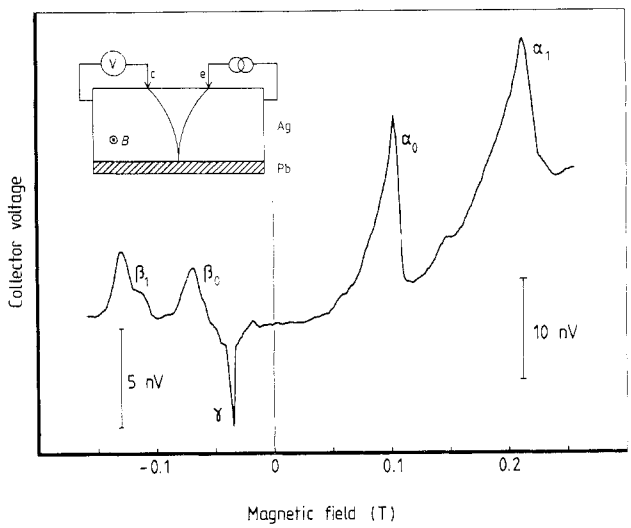

Figure 17. Measured collector voltage on a Ag(0 0 1) surface in a TEF experiment as a function of applied magnetic field. The α-peaks indicate focusing of electrons on belly orbits, the β-peaks of electrons on four-cornered-rosette orbits. The γ-peak detects the focusing of holes, originating from Andreev reflections of electrons at the Ag–Pb interface. The inset shows the experimental set-up with an example of a trajectory of an Andreev-reflected quasi-particle from the emitter to the collector in the presence of a magnetic field.

possible to observe directly the Andreev reflection of electrons on a normal metal–superconductor interface.

Recently the method has been used to study the energy dependence of the electron–phonon interaction. Compared with the traditional point-contact experiments on this interaction, an advantage is that in the double-point-contact experiments the interaction can be studied on a specific orbit of the Fermi surface.

The technique of transverse electron focusing (TEF) can be understood easily. As we already mentioned, electrons are injected into the metal by the emitter point contact. A homogeneous magnetic field, parallel to the crystal surface, forces these electrons onto paths in real space that are just the orbits in k-space but rotated over 90° and scaled with a factor $\hbar/eB$. The electrons follow paths over the Fermi surface perpendicular to the field direction and return to the surface at a certain distance from the point of injection, depending on the strength of the applied magnetic field. The electrons are injected into all directions, but focusing takes place at a distance $2\hbar k_F/eB$ from the emitter.

For the case of specular reflection on the surface, focusing also occurs at multiples of this distance from the emitter. Figure 17 shows the observed collector voltage on a Ag(0 0 1) surface as a function of the magnetic field. For the chosen crystal orientation with respect to the magnetic field, focusing of the electrons on belly orbits (peaks α_0, α_1) and on four-cornered-rosette orbits (peaks β_0, β_1) can be observed. The peak α_0 (β_0) corresponds to the direct focusing and α_1 (β_1) after one reflection. From the relative intensity of successive peaks a study can be made of the internal reflectivity of the Ag surface (Benistant *et al* 1986). The electrons on the rosette orbits (β_0, β_1) are seen at negative fields because the effective mass of the electrons on these orbits

is negative, resulting in an opposite rotation of the electrons in a magnetic field compared to the belly orbits.

Transverse electron focusing has been applied to investigate the Andreev reflection of electrons at the interface between a normal metal and a superconductor (Bozhko *et al* 1982, Benistant *et al* 1983). An Andreev reflection describes the process of an electron passing from a normal to a superconducting metal. The traversing electron condenses into the superconducting state by forming a Cooper pair with another electron, withdrawn from the normal metal. Because of mass, charge and momentum conservation, a quasi-particle with opposite mass, group velocity and charge, i.e. a hole, will come back from the interface into the normal metal. A direct observation of the Andreev reflection can be made by evaporating a superconducting film on the Ag surface opposite to the surface where the emitter and collector are placed. In the inset of figure 17 an example of an Andreev-reflected quasi-particle is given in the presence of a magnetic field. In the same figure the γ-peak detects the focusing of the holes originating from an Andreev reflection. The amplitude of the γ-peak is opposite to the other peaks because of the opposite charge of the quasi-particles. Andreev reflection was also observed in an experiment with a single point contact on a thin Ag crystal with a Pb film evaporated at the opposite side (Benistant *et al* 1985). This single point contact served both as emitter and as collector in the experiment. Because of the retro-reflection of the quasi-particles at the surface between superconductor and normal metal, the Andreev-reflected quasi-particles return exactly at the place of ballistic injection. The voltage-dependent resistance of the single contact shows a minimum for voltages below the superconducting gap, where Andreev reflections are possible. With this experiment the energy dependence of the Andreev reflection has been investigated by measuring the voltage-dependent contact resistance.

A more recent experiment in which TEF between two point contacts was used is that of van Son *et al* (1987) in which the electron–phonon interaction is studied. In this study the magnetic field was tuned at a value B_0 for electron focusing to occur. At this field the decrease of the focusing peak was measured with increasing energy of the emitted electrons. The focusing-peak height P will be a function of the emitter voltage via

$$P(eV) = P(0)\exp[-t/\tau(eV)] \tag{24}$$

in which $\tau(eV)$ is the energy-dependent scattering time of the electrons and $t = \pi m/eB_0$ is the time during which the electrons travel from the emitter to the collector. For $T = 0$ the electron–phonon scattering time is given by (equation (5))

$$\frac{1}{\tau(\varepsilon, T=0)} = 2\pi \int_0^{\varepsilon/\hbar} \mathrm{d}\omega\, \alpha^2 F(\omega) \simeq b\varepsilon^3. \tag{25}$$

Here $\alpha^2 F(\omega)$ is the Eliashberg function, which for low energies may be approximated by a quadratic energy dependence. The coefficient b depends on crystal direction. Thus using the effects of TEF it is possible to measure the anisotropy in this coefficient. This is a great advantage of this method compared with the normal point-contact spectroscopy in which an average is taken over all possible crystal directions. Figure 18 shows the measured TEF signal as a function of applied emitter voltage for an experiment on the (1 0 0) surface of Ag with the magnetic field pointing along the [0 0 1] direction. Clearly visible is the decrease in signal when the electron energy is increased due to the increasing scattering rate $1/\tau$ of the electrons along their path. At higher voltages a background signal arises with even a second maximum at

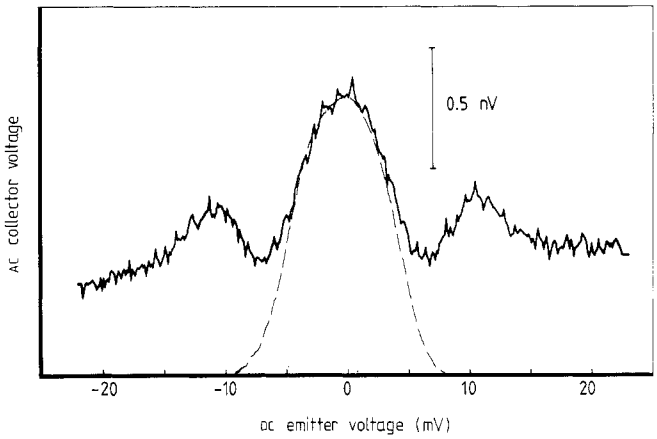

Figure 18. Measured AC collector voltage as a function of applied emitter voltage for a TEF experiment on the (1 0 0) surface of Ag with the magnetic field in the [0 0 1] direction, showing the decrease of signal at increasing emitter voltage due to an increase of scattering of the electrons along their trajectory. The broken curve is the theoretical TEF signal, calculated with equations (24) and (25).

approximately 12 mV. The background can be ascribed to electrons which scatter close to the emitter into the direction of the focusing orbit. The maximum at about 12 mV coincides approximately with the maximum which is observed in traditional point-contact spectra. The broken curve in figure 18 is the calculated voltage dependence of the TEF signal, using equations (24) and (25) with b as fitting parameter. By measuring the focusing signal at different crystal orientations, van Son *et al* (1987) investigated the anisotropy in the electron–phonon scattering.

7.4. Noise in point contacts

Because of the small dimensions of point contacts, $1/f$ noise is the dominant type of noise observed for frequencies up to a few kilohertz. According to Hooge's empirical formula for the power density of this noise ($S_V = \alpha V^2/Nf$ (Hooge and Hoppenbrouwers 1969), where α is a constant and N is the total number of charge carriers), this $1/f$ noise becomes more important when the number of charge carriers in the fluctuating system is decreased, for instance in semiconducting systems or in systems with very small dimensions, e.g. point contacts. For a contact the total number of charge carriers is given by the product of the electron density n and the contact volume a^3.

Measurements on Na, Cu and Ni indeed show this quadratic voltage dependence for contacts in the dirty limit (Akimenko *et al* 1984b) at low voltages. For higher voltages deviations occur. Also contacts in the ballistic regime exhibit noise spectra which correspond well with Hooge's formula. However, in these spectra, an additional structure is observed in the voltage range of the phonon frequencies. The noise spectra reveal features, not always exactly reproducible, but much sharper and more detailed than in the usual point-contact spectra. A correlation of the maxima and minima in the spectra is found with specific umklapp and normal scattering processes in the electron–phonon interaction.

7.5. Generation of phonons with metallic point contacts and their detection

In § 3.1 we discussed the background that is often present in the measured phonon spectra. An explanation for this background is the existence of non-equilibrium phonons in the systems and subsequent additional scattering of conduction electrons with these non-equilibrium phonons. Thus in the case of ballistic contacts, we have both electron and phonon systems that are not in equilibrium. So far most experiments on point contacts have dealt with the non-equilibrium electron distribution which is the reason for most electrical and thermal non-linearities. Recently some experiments have been performed in which the generated phonon system was studied. A bottleneck in all these experiments is the fact that the phonons which are generated by the point contact have to travel through a metal film and pass the boundary between this metal film and an insulator or semiconductor in which detection takes place. In this transport of phonons from the contact area, extra scattering of these phonons can take place, resulting in possible thermalisation of the phonon system. Thus both film thickness and boundary have to be controlled very carefully in the experiments.

The non-equilibrium phonon distribution for a ballistic point contact is given by (Jansen *et al* 1980)

$$N(\varepsilon, eV) = \begin{cases} 0.32[(eV - \varepsilon)/\varepsilon]\, a/l_p(\varepsilon) & (\varepsilon \leqslant eV) \quad (26a) \\ 0 & (\varepsilon \geqslant eV) \quad (26b) \end{cases}$$

where $l_p(\varepsilon)$ is the energy-dependent phonon mean free path and V is the applied bias voltage over the contact. A striking feature of this phonon distribution is the cut-off at a phonon energy $\varepsilon = eV$. In the case of a normal heater or whenever the phonon system is thermalised, one has a Bose distribution of phonons which is then given by

$$N(\varepsilon, T) = [\exp(\varepsilon/k_B T) - 1]^{-1}. \quad (27)$$

This distribution still has a non-zero value for high phonon energies, i.e. up to the Debye energy. In general the temperature T in such a thermal phonon distribution depends on the applied voltage V. For instance in the case of a point contact in the dirty regime this dependence is just given by equation (8).

In an experiment by Goossens *et al* (1984) the phonon distribution in a point-contact configuration was studied using a fluorescence experiment in ruby. By measuring the R_2 fluorescence, ruby can be used as a detector that is sensitive to phonons with an energy of 3.6 meV. The phonons were generated in a point contact which was made between a Au whisker and a Au film, evaporated on the ruby. The phonon detection was not sensitive enough to detect any signal around an applied voltage of 3.6 mV, where a threshold in the detected signal was expected. For higher applied voltages it was concluded that the point contact acts as a Planck radiator ($P \propto T_{\text{eff}}^4$).

In another experiment an attempt was made to distinguish between the non-equilibrium distribution (equation (26)) and the thermal phonon distribution (equation (27)). Here a thin gold film of 40 nm thickness was evaporated on a silicon crystal with thickness 3 mm, which was doped with boron impurities. These boron impurities supply a phonon detection mechanism. By illumination with visible light, one creates electron–hole pairs in the silicon. The boron impurities can bind such a hole, forming a B^+ impurity with an ionisation energy of 2.0 meV. Phonons with an energy larger than this ionisation energy neutralise the acceptors, yielding extra holes in the valence band of the Si and hence increasing its conductivity. A more detailed description of the B-doped Si as a phonon detector can be found in publications by Burger and Lassmann (1984, 1986).

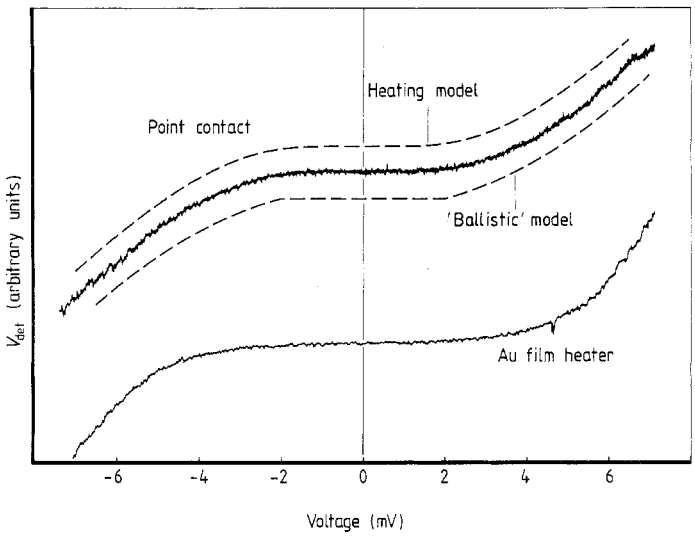

Figure 19. Measured phonon-induced conductivity signal in Si with a Au point contact (upper full curve) and a Au film (lower full curve) as phonon generator, as a function of applied bias voltage over the generator. The point contact was made between a Au whisker and a Au film, evaporated on the Si crystal. The broken curves are calculated signals using the heater model (upper broken curve) and a ballistic-contact model (lower broken curve).

In the evaporated gold film, phonons were generated with a point contact. After travelling through the Au–Si interface and through the Si sample, these phonons were detected with phonon-induced conduction at the opposite side of the Si sample. Figure 19 gives an example of the detected signal as a function of bias voltage over the point contact.

Assuming that the observed conduction enhancement is directly proportional to the number of phonons present in the Si, one can write for the measured signal

$$V_{\text{det}} \propto \frac{\mathrm{d}}{\mathrm{d}V} \int_{\varepsilon_c}^{\varepsilon_D} N(\varepsilon) F(\varepsilon)\, \mathrm{d}\varepsilon. \tag{28}$$

Here ε_c is the threshold energy above which the phonons give a contribution, i.e. it is the ionisation energy of the B^+ impurities (2 meV), ε_D is the Debye energy, $N(\varepsilon)$ is the phonon distribution function and $F(\varepsilon)$ is the phonon density of states, which in the Debye approximation is $F(\varepsilon) \propto \varepsilon^2$. The voltage derivative in equation (28) appears because the measurements were performed with a lock-in technique.

In figure 19 this calculated signal is represented by the broken curves using the phonon distribution of a heater (upper broken curve) and of a ballistic contact (lower broken curve). Although the two broken curves are very similar, the derivative signal $\mathrm{d}V_{\text{det}}/\mathrm{d}V$, which was also measured, is better described with the thermalised phonon distribution of a heater. For this heater model, the heater temperature was related to the applied voltage as for a Planck radiator, i.e. $T^4 = T_{\text{bath}}^4 + \alpha^2 V^2$, where α is given by the matching for the phonons between the heater (i.e. the hot spot in the Au film) and the Si crystal (Weis 1969, Rösch and Weis 1977). In the same figure also the measured signal is drawn for the case where the Au film was used as a uniform heater.

Assuming that the point contact acts as a heater, the factor α which links temperature with voltage can be obtained by comparing the measured signals with the

calculated ones. The theory for the matching between a Au film and a Si crystal predicts a value of α according to $\alpha^4 AR = 6.3 \times 10^{-3}\,\mathrm{K^4\,m^2\,s\,J^{-1}}$, in which A is the area of the hot surface and R the heater resistance. Applying this to the experimental results of the point contact, one finds a hot area of $\sim 200 \times 200\ \mu\mathrm{m}^2$, much larger than one would expect by comparison with the contact diameter (~ 10 nm) or the inelastic electron mean free path ($\sim 1\ \mu$m).

From the experiments it can be concluded that a threshold at $eV = \varepsilon_c$ is not observed. Besides, the measured signals are very well described with a heater model; however, this leads to an unexpectedly large hot area. That a 'ballistic' phonon distribution is not observed is probably due to acoustic mismatch between the gold film and the silicon, preventing most of the phonons from entering the crystal. Therefore most likely a thermalisation of the phonon system takes place, leading to a 'normal heater' phonon distribution.

8. Concluding remarks

Nowadays, in most more or less simple metals, metallic point contacts can be used as a standard technique for the spectroscopic investigation of the energy-dependent inelastic scattering of electrons in the metal. In particular, the electron–phonon interaction has been studied in detail in very many metals with the point-contact technique, and quantitative comparisons have been made with other experimental techniques (e.g. inelastic neutron scattering) and theoretical band-structure calculations for the determination of the strength of the interaction for the different phonon branches. Point-contact spectroscopy can be applied for the study of the interaction of the electrons with other excitations in a metal as well (e.g. magnons, paramagnetic impurities, crystal-field levels, etc.), but again the technique seems to be limited at present to more or less simple metals. The essential restriction in the use of point contacts as a spectroscopic tool is given by the condition that the contact diameter (typically 10 nm) has to be smaller than the energy-dependent scattering length $l_i(eV)$. This inelastic length has to be seen as the relaxation length for a non-equilibrium electron with energy eV above the Fermi level in a cold environment with the same temperature as the surrounding bath. As a direct consequence of this dimensional condition, the relative resistance change $\Delta R(V)/R$ of the voltage-dependent contact resistance has to be smaller than unity in a point-contact experiment in order to give reliable spectroscopy information, because $\Delta R(V)/R \simeq a/l_i(eV)$. This relation holds for both the ballistic and diffusive regimes. Most unfortunately, in non-simple but interesting and fascinating metals (valence fluctuators, heavy-fermion systems, etc.), this relation is not always fulfilled; therefore, the analysis of point-contact experiments with these metals is far from straightforward and unambiguous. More work has to be done until these problems are solved satisfactorily.

More elaborate configurations of point-contact experiments allow the study of all sorts of transport problems in metals. With a double-point-contact set-up, electron-focusing experiments allow the study of the inelastic scattering of electrons along specific orbits in single crystals selected by a magnetic field. The influence of various parameters (magnetic field, temperature gradients) in a point-contact experiment leads to particular phenomena (diffraction of electron wavefunction at a small constriction, quenching of phonon drag at a small contact). Several properties (electrical noise, video response, phonon generation) of a point contact with small dimensions are

related to interesting aspects in surprisingly many subfields of solid-state physics (origin of $1/f$ noise, timescale of scattering processes, non-equilibrium distributions). The recent discovery of ballistic transport through point contacts in two-dimensional systems (van Wees *et al* 1988, Wharam *et al* 1988), where the quasi-classical approach of the Boltzmann equation is no longer valid, and the advances in the techniques of the scanning tunnelling microscope seem to open entirely new avenues for point-contact spectroscopy.

Acknowledgments

Part of this work has been supported by the Stichting voor Fundamenteel Onderzoek der Materie (Foundation for Fundamental Research on Matter) with financial support from the Nederlandse Organisatie voor Zuiver Wetenschappelijk Onderzoek (Netherlands Organisation for the Advancement of Pure Research).

References

Akimenko A I, Ponomarenko N M, Yanson I K, Janos S and Reiffers M 1984a *Fiz. Tverd. Tela* **26** 2264 (Engl. Transl. 1984 *Sov. Phys.–Solid State* **26** 1374)

Akimenko A I, Verkin A B, Ponomarenko N M and Yanson I K 1982 *Fiz. Nizk. Temp.* **8** 1084 (Engl. Transl. 1982 *Sov. J. Low Temp. Phys.* **8** 547)

Akimenko A I, Verkin A B and Yanson I K 1984b *J. Low Temp. Phys.* **54** 247

Balkashin O P, Yanson I K, Solov'ev V S and Krasnogotov A Yu 1982 *Zh. Tekh. Fiz.* **52** 811 (Engl. Transl. 1982 *Sov. Tech. Phys.* **27** 522)

Barnard R D 1972 *Thermoelectricity in Metals and Alloys* (London: Taylor and Francis)

Benistant P A M, van de Walle G F A, van Kempen H and Wyder P 1986 *Phys. Rev.* B **33** 690

Benistant P A M, van Gelder A P, van Kempen H and Wyder P 1985 *Phys. Rev.* B **32** 3351

Benistant P A M, van Kempen H and Wyder P 1983 *Phys. Rev. Lett.* **51** 817

Bogachek E N, Kulik I O and Shekhter R I 1985a *Solid State Commun.* **56** 999

Bogachek E N, Kulik I O and Shkorbatov A G 1985b *Fiz. Nizk. Temp.* **11** 1189 (Engl. Transl. 1985 *Sov. J. Low Temp. Phys.* **11** 656)

Bozhko S I, Tsoi V S and Yakovlev S E 1982 *Pis. Zh. Eksp. Teor. Fiz.* **36** 123 (Engl. Transl. 1982 *JETP Lett.* **36** 152)

Burger W and Lassmann K 1984 *Phys. Rev. Lett.* **53** 2035

—— 1986 *Phys. Rev.* B **33** 5868

Bussian B, Frankowski I and Wohlleben D 1982 *Phys. Rev. Lett.* **49** 1026

d'Ambrumenil N and White R M 1982 *J. Appl. Phys.* **52** 2052

Duif A M, Jansen A G M, Wyder P and d'Ambrumenil N 1987 to be published

Frankowski I and Wachter P 1982 *Solid State Commun.* **41** 577

Goossens R J G, Dijkhuis J I, de Wijn H W, Jansen A G M and Wyder P 1984 *Physica* B **127** 422

Harrison W A 1961 *Phys. Rev.* **123** 85

Holm R 1967 *Electric Contacts* (Berlin: Springer)

Hooge F N and Hoppenbrouwers A M H 1969 *Phys. Lett.* **29A** 642

Jansen A G M, Duif A M, Lysykh A A and Wyder P 1988 *Narrow Band Phenomena—Influence of Electrons with both Band and Localised Character* (NATO Advanced Study Workshop) ed. J C Fuggle, G Sawatzky and J W Allen (New York: Plenum)

Jansen A G M, van Gelder A P and Wyder P 1980 *J. Phys. C: Solid State Phys.* **13** 6073

Knudsen M 1934 *Kinetic Theory of Gases* (London: Methuen)

Kulik I O, Omel'yanchuk A N and Shekhter R I 1977 *Fiz. Nizk. Temp.* **3** 1543 (Engl. Transl. 1977 *Sov. J. Low Temp. Phys.* **3** 740)

Kulik I O and Shekhter R I 1980 *Fiz. Nizk. Temp.* **6** 184 (Engl. Transl. 1980 *Sov. J. Low Temp. Phys.* **6** 88)

Kulik I O and Yanson I K 1978 *Fiz. Nizk. Temp.* **4** 1267 (Engl. Transl. 1978 *Sov. J. Low Temp. Phys.* **4** 596)
Kunii S 1987 *J. Magn. Magn. Mater.* **63 + 64** 673
Lifshitz I M, Azbel' M Ya and Kaganov M I 1956 *Zh. Eksp. Teor. Fiz.* **31** 63 (Engl. Transl. 1957 *Sov. Phys.–JETP* **4** 41)
Lysykh A A, Duif A M, Jansen A G M and Wyder P 1988a to be published
Lysykh A A, Duif A M, Jansen A G M, Wyder P and de Visser A 1988b *Phys. Rev.* B **38** 1067
Lysykh A A, Yanson I K, Shklyarevskii O I and Naidyuk Yu G 1980 *Solid State Commun.* **35** 987
McMillan W L and Rowell J M 1965 *Phys. Rev. Lett.* **14** 108
Maxwell J C 1904 *A Treatise on Electricity and Magnetism* (Oxford: Clarendon)
Moser M, Wachter P and Franse J J M 1986 *Solid State Commun.* **58** 515
Moser M, Wachter P, Hulliger F and Etourneau J R 1985 *Solid State Commun.* **54** 241
Naidyuk Yu G, Gribov N N, Lysykh A A, Yanson I K, Brandt N B and Moshchalkov V V 1985a *Pis. Zh. Eksp. Teor. Fiz.* **41** 325 (Engl. Transl. 1985 *JETP Lett.* **41** 399)
Naidyuk Yu G, Gribov N N, Shklyarevskii O I, Jansen A G M and Yanson I K 1985b *Fiz. Nizk. Temp.* **11** 1053 (Engl. Transl. 1985 *Sov. J. Low Temp. Phys.* **11** 580)
Paulus E and Voss G 1985 *J. Magn. Magn. Mater.* **47 + 48** 539
Pearson W B 1961 *Solid State Phys. (USSR)* **3** 1411
Pepper M 1980a *J. Phys. C: Solid State Phys.* **13** L709
—— 1980b *J. Phys. C: Solid State Phys.* **13** L717
—— 1980c *J. Phys. C: Solid State Phys.* **13** L721
Pong-Fei Lu, Tsui D C and Cox H M 1985 *Phys. Rev. Lett.* **54** 1563
Reiffers M, Flachbart K and Janos S 1986 *Pis. Zh. Eksp. Teor. Fiz.* **44** 232 (Engl. Transl. 1986 *JETP Lett.* **44** 298)
Rösch F and Weis O 1977 *Z. Phys.* B **27** 33
Sharvin Yu V 1965 *Zh. Eksp. Teor. Fiz.* **48** 984 (Engl. Transl. 1965 *Sov. Phys.–JETP* **21** 655)
Sharvin Yu V and Fisher L M 1965 *Pis. Zh. Eksp. Teor. Fiz.* **1** 54 (Engl. Transl. 1965 *JETP Lett.* **1** 152)
Shen L Y L and Rowell J M 1968 *Phys. Rev.* **165** 566
Shklyarevskii O I, Jansen A G M, Hermsen J G H and Wyder P 1986a *Phys. Rev. Lett.* **57** 1374
Shklyarevskii O I, Jansen A G M and Wyder P 1986b *Fiz. Nizk. Temp.* **12** 947 (Engl. Transl. 1986 *Sov. J. Low Temp. Phys.* **12** 536)
Swartjes H M, Jansen A G M and Wyder P 1988a *Phys. Rev.* B **38** 8114
Swartjes H M, van Gelder A P, Jansen A G M and Wyder P 1988b to be published
Tien P K and Gordon J P 1963 *Phys. Rev.* **129** 647
Trzcinski R, Gmelin E and Queisser H J 1986 *Phys. Rev. Lett.* **56** 1086
Tsoi V S 1974 *Zh. Eksp. Teor. Fiz. Pis. Red.* **19** 114 (Engl. Transl. 1974 *JETP Lett.* **19** 70)
van Gelder A P 1980 *Solid State Commun.* **35** 19
van Gelder A P, Jansen A G M and Wyder P 1980 *Phys. Rev.* B **22** 1515
van der Heijden R W, Jansen A G M, Stoelinga J H M, Swartjes H M and Wyder P 1980 *Appl. Phys. Lett.* **37** 245
van der Heijden R W, Swartjes H M and Wyder P 1984 *Phys. Rev.* B **30** 3513
van Son P C, van Kempen H and Wyder P 1987 *Phys. Rev. Lett.* **58** 1567
van Wees B J, van Houten H, Beenakker C W, Williamson J G, Kouwenhoven L P, van der Marel D and Foxon C T 1988 *Phys. Rev. Lett.* **60** 848
Verkin B I, Yanson I K, Kulik I O, Shklyarevskii O I, Lysykh A A and Naidyuk Yu G 1980 *Izv. Akad. Nauk SSSR, Ser. Fiz.* **44** 1330
Weis O 1969 *Z. Angew. Phys.* **26** 325
Wexler G 1966 *Proc. Phys. Soc.* **89** 927
Wharam D A, Thornton T J, Newbury R, Pepper M, Ahmed H, Frost J E F, Hasko D G, Peacock D C, Ritchie D A and Jones G A C 1988 *J. Phys. C: Solid State Phys.* **21** L209
Yanson I K 1974 *Zh. Eksp. Teor. Fiz.* **66** 1035 (Engl. Transl. 1974 *Sov. Phys.–JETP* **39** 506)
—— 1983 *Fiz. Nizk. Temp.* **9** 676 (Engl. Transl. 1983 *Sov. J. Low Temp. Phys.* **9** 343)
Yanson I K and Shklyarevskii O I 1986 *Fiz. Nizk. Temp.* **12** 899 (Engl. Transl. 1986 *Sov. J. Low Temp. Phys.* **12** 509)